Title
ELECTRON IMPACT DISSOCIATION OF IRON PENTACARBONYL AND FORMATION OF THIN FILMS

Author
Hale, B.C.

Publication Date
1983

Lawrence Berkeley Laboratory
UNIVERSITY OF CALIFORNIA

Materials & Molecular
Research Division

ELECTRON IMPACT DISSOCIATION OF IRON PENTACARBONYL AND FORMATION OF THIN FILMS

Brian Carleton Hale
(Ph.D. Thesis)

January 1983

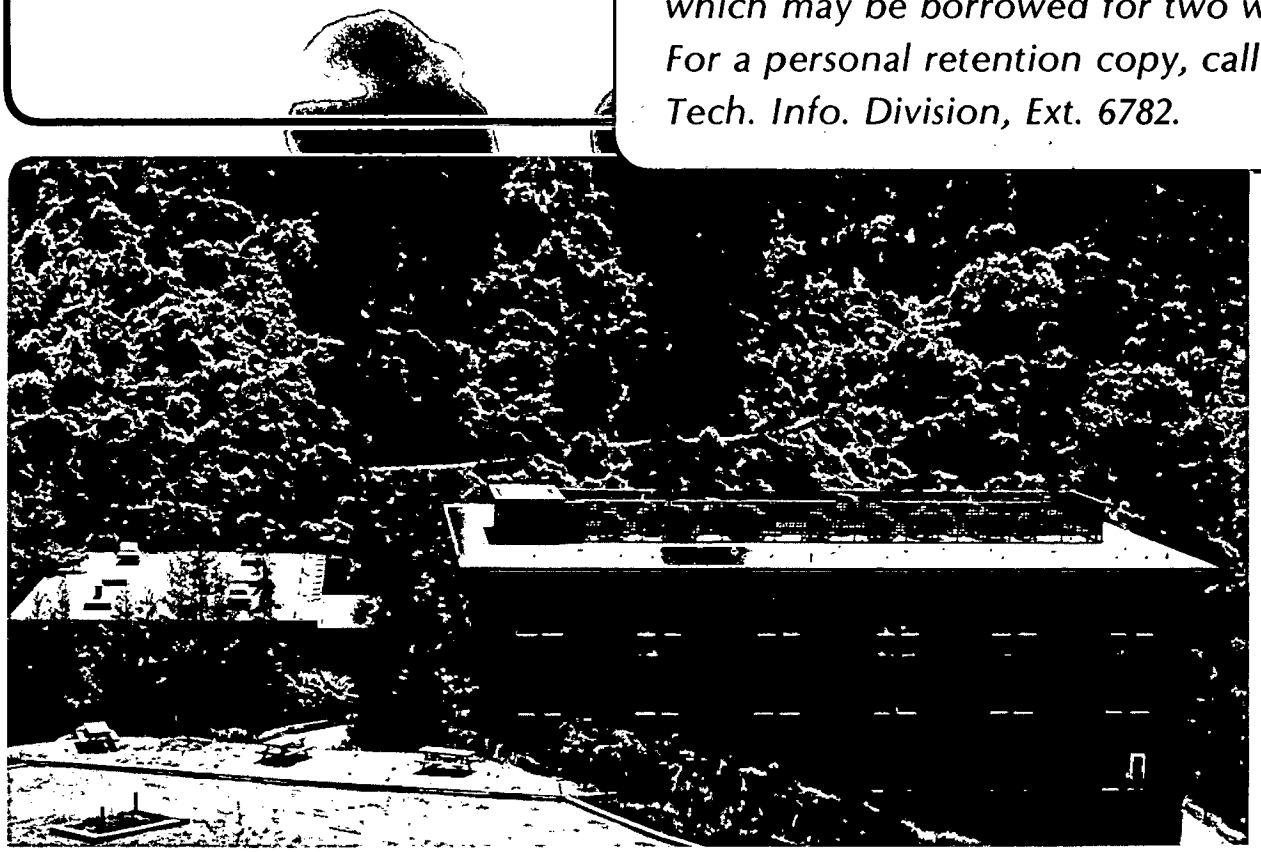

Prepared for the U.S. Department of Energy under Contract DE-AC03-76SF00098

DISCLAIMER

LBL # 15708

Electron Impact Dissociation of Iron Pentacarbonyl and Formation of Thin Films

Brian Carleton Hale

Materials and Molecular Research Division
Lawrence Berkeley Laboratory

and

Department of Chemistry
University of California
Berkeley, CA 94720

ABSTRACT

A quantitative study of the fluorescence yield from electron impact dissociation of $Fe(CO)_5$ in a semi-effusive beam was carried out and compared favorably with a limited degree of freedom statistical dissociation model for an excitation energy of 100 eV. An absorption cross-section was measured to be 4.7 $\mathring{A}^2 \pm 0.4\ \mathring{A}^2$. A quantum fluorescence yield was measured to be 2×10^{-4} at an electron energy of 100 eV.

Thin iron films were formed from $Fe(CO)_5$ on glass surfaces using a Mercury/Xenon high pressure arc lamp. The kinetics of this process were studied by measuring the increase in pressure due to the dissociation of $Fe(CO)_5$. The rate of dissociation closely followed the rate equation for dissociation by both photolysis and electron dissociative attachment due to low energy electrons emitted by the surface.

ACKNOWLEDGMENTS

I would like to thank John Winn for his ideas and guidance in this research. Thanks, also, to the rest of the "Awesome Winn Group", Dennis, Jim, Dave, Mike, Sue, Henry and Will, for their suggestions, stimulation and humor. A special thanks to Dave Horak for his direct participation in the fluorescence experiments without which would not have been possible.

Thanks to Jim Roe, Barrett Bobsein, Wayne Glad, Tony O'Keefe, Mike Maier, Mike Simonson, the "Awesome Winn Group" (again) and Anheuser-Bush for making my stay at Berkeley most interesting.

This work was supported by the Director, Office of Energy Research, Office of Basic Energy Sciences, Chemical Sciences Division of the U.S. Department of Energy under Contract No. DE-AC03-76SF00098.

Finally, I wish to give my greatest thanks to Terri for her patience, moral support, encouragement and devotion.

TABLE OF CONTENTS

Chapter I

INTRODUCTION

There are various methods for dissociating metal carbonyls producing gaseous bare metal atoms. Thermal decomposition[1,2] provides a relatively easy means of dissociating metal carbonyls. Photolysis[3,4,5] has also been used to dissociate metal carbonyls and at the same time induce excitation of the metal atom. Quenching[6] of metastable rare gases by metal carbonyls is a relatively new method for dissociating metal carbonyls. This process also allows excitation of the metal atom. Experimental evidence has indicated that this metastable dissociative process is a single bimolecular energy transfer followed by simultaneous dissociation of the ligands from an excited metal atom.

The present work uses electron impact as a means of dissociating $Fe(CO)_5$ leaving excited iron atoms. Comparison of the fluorescence spectra obtained by this process with the chemiluminescence spectra obtained by Hartman[6] and Horak[5] gave an indication of the mechanism involved.

One side effect of all these dissociative processes is the formation of metal films on surfaces. Baker and Bernstein[1] used thermal decomposition of nickel carbonyl to form thin nickel films on Pyrex glass. They found these films to be active hydrogen catalysts. Nagy et al.[7] formed iron films using both thermal and photochemical decomposition of $Fe(CO)_5$.

Another aspect of the present work was the use of the photoelectric effect to emit electrons from the surface of soda glass. It is believed that the electrons, through dissociative attachment, form fragmented neg-

ative ions i.e.,

$$Fe(CO)_5 + e^- \rightarrow Fe(CO)_{5-n}^- + CO_n \qquad n=1,2,3,4,5 \qquad (I-1)$$

These ions are then attracted to the surface where further dissociation and neutralization occurs. By monitoring the rate of dissociation of $Fe(CO)_5$ for this process, the rate law can be obtained. This rate law will be shown to be in good agreement with the above mechanism.

REFERENCES FOR CHAPTER I

1. L.L. Baker, Jr., and R.B. Bernstein, J. Am. Chem. Soc., 73, 4434 (1951).
2. S.M. Schilderout, G.A. Pressley, Jr., and F.E. Stafford, J. Am. Chem. Soc., 87:7, 1617 (1967).
3. Z. Karny, R. Naaman, and R.N. Zare, Chem. Phys. Lett., 59, No. 1, 33 (1978).
4. L. Hellner, J. Masanet, and C. Vermeil, Nouveau Journal De Chimie, 3, 721 (1979).
5. D.V. Horak, Ph.D. Thesis, University of California, Berkeley, LBL Report 14612 (1982).
6. D.C. Hartman, Ph.D. Thesis, University of California, Berkeley, LBL Report 9819 (1980).
7. J.B. Nagy, M. van Eenoo, and E.G. Derouane, J. of Cat., 58, 230 (1979).

Chapter II

ELECTRON IMPACT DISSOCIATION OF IRON PENTACARBONYL

The electron impact dissociation of $Fe(CO)_5$ was studied by observing the fluorescence of Fe^* when a beam of $Fe(CO)_5$ was crossed with a beam of electrons. A block diagram of the apparatus is shown in Fig. II-1.

Briefly, an effusive beam of $Fe(CO)_5$ was formed through a 1/4 in. diameter opening into the interaction chamber. A variable energy electron gun generated a beam of electrons which crossed the $Fe(CO)_5$ beam at a right angle. A Faraday cup at the opposite side of the chamber from the electron gun monitored the emission current. The total visible and near UV fluorescence was collected by a photomultiplier (PMT) located behind a quartz window placed orthogonal to both the $Fe(CO)_5$ and the electron beams. A 0.25 monochromator was placed between the PMT and the quartz window to collect the dispersed fluorescence in certain experiments. The PMT was operated in a pulse counting mode. Discriminated PMT pulse were counted by standard electronics and accumulated under control of a Commodore PET 2001 microcomputer. The interaction chamber and data collection system were designed by Dr. David V. Horak[1]. A more detailed discussion of the appartus follows.

A. Interaction Chamber

Electron impact dissociation of $Fe(CO)_5$ was first attempted in a flow system. Approximately 30 torr of $Fe(CO)_5$ was flowed through a 1/4 in. stainless steel tube into a ca. 2 1/2 in. diameter tee-shaped chamber. An electron beam generated from an electron gun was set orthogonal

to the flow of $Fe(CO)_5$ vapor. One major problem developed from this system. Iron from dissociated $Fe(CO)_5$ plated out on the filament, reducing the emission current to ca. zero and eventually caused the filament to burn open. All this would occur approximately 10 to 20 seconds after turning on the $Fe(CO)_5$ flow. For this reason, it was deemed necessary to collimate the $Fe(CO)_5$ as a molecular beam.

The interaction chamber, Fig. II-2, was a 13 in. X 15 in. X 13 in. rectangular box constructed out of 1/2 in. thick 304 stainless steel. A glass bulb (sample reservoir) was connected to a 1 in. O.D. brass tube which was fed through the top of the interaction chamber using a Cajon o-ring quick couple. The sample reservoir was immersed in a water bath which was maintained at a constant temperature of 15°C. The end of the brass tube could be fitted with various size nozzles which produced a semi-effusive beam. No further collimation was used. A solenoid valve set approximately 4 in. above the nozzle was used to turn the beam on and off.

Inside the interaction chamber was a copper LN_2 reservoir and four cooled copper baffles. These allowed the entire chamber to be cryopumped, minimizing the amount of $Fe(CO)_5$ entering the electron gun. A further discussion of this will be given in the section on the electron gun. The chamber was pumped by a 700 1/sec. CVC 4 in. diffusion pump backed by a Welch 1402 mechanical pump. The chamber could be pumped down to ca. 2×10^{-7} torr. The entire inside of the chamber was painted black in order to decrease the amount of scattered light from the electron gun.

B. Fluorescence Monitoring

The fluorescence was observed through a 2 1/2 in. diameter quartz

window supported by a 6 in. flange orthogonal to both the $Fe(CO)_5$ and the electron beams. This window was periodically cleaned with HCl to remove any metallic iron which plated out on its surface. On the outside of the flange supporting the window was a 6 in. long light tight tube housing an EMC9824B PMT. The PMT high voltage was set at -1600V using a PAR 1105 data converter as its power source. The signal from the PMT was fed through a PAR 1120 discriminator to the data converter. The output of the data converter was ECL type pulses which were fed to an ECL to TTL converter. The TTL pulses were counted by a Commodore PET computer. The counting software was provided by David V. Horak[1].

C. Electron Gun

The electron beam was generated by a modified Pierce electron gun. The electron beam was focused through the center of the reaction chamber into a Faraday cup supported by an LN_2 baffle on the opposite side of the chamber. The Faraday cup monitored the electron beam current throughout the experiments. The electron gun produced a stable electron beam current of 10^{-7} amps using a 0.003 in. diameter 2% thoriated tungsten filament run at 3 amps and ca. 1.5 volts under the most ideal conditions i.e., no $Fe(CO)_5$ introduced into the system. The energy of the beam could be changed from approximately 60 volts to 180 volts with no significant change in the beam current.

Because of the nature of the experiment two problems had to be considered when designing the electron gun. First, since photons from the fluorescence of Fe^* were to be observed, the amount of light emitted by the electron gun had to be small in comparison. Second, the amount of Fe allowed to contaminate the filament had to be minimized in order to

maintain a stable electron beam current. The first problem was solved by designing light tight shields used in the construction of the electron gun. The second and more difficult problem was minimized by collimating the $Fe(CO)_5$ and by allowing the electron gun mounting assembly to be cooled to LN_2 temperature.

The electron gun, Fig.II-3, was cylindrically symmetric about the electron beam axis. The gun could be assembled and placed into the mount, Fig. II-4, as a unit. The gun was assembled by screwing four #4-40 threaded rods into the light shield. A teflon light tight ring was then fitted snugly into the light shield. The final focusing stage, two grids, filament shield and back plate were electrically isolated and accurately spaced by 3/16 in. diameter ceramic balls which fit in 120° dimples drilled 3/64 in. deep in each of these elements. The four threaded rods went through the back plate and held the assembly together with four nuts. The filament holder was made of boron nitride and fitted snugly into the filament shield. The thoriated tungsten filament was spot welded to two stainless steel posts which were mounted in the filament holder.

Fig. II-5, shows a block diagram of the electron gun controls. The filament power supply was floated on the filament shield power supply (filament float) which allowed the electrons to be generated at the potential of the filament float i.e., the electron beam energy was determined by the filament float. Although the float could be varied from 0 to -180 volts, the electron beam current dropped to about 10^{-9} amps in the range of 0 to -30 volts. For this reason, the float was limited to the range of -50 to -180 volts. In order to vary the electron beam energy and not significantly change the focusing conditions (or, more impor-

tantly, the electron beam current) both grids and the final focusing stage were also floated on the filament float. When the electron beam energy was changed from 50 volts to 180 volts, the beam current dropped approximately 70 per cent. However, this could be corrected by adjusting the final focusing stage voltage slightly, ca. 5 to 10 volts. The filament emission current was measured at the first grid to be 10^{-6} amps while the current measured at the Faraday cup was 10^{-7} amps indicating less than 10 per cent of the electrons generated at the filament were focused into the Faraday cup. The first grid could also be used to pulse the electron beam off by applying a large negative (~-200 v) pulse to it. Typical operating conditions are shown in Table II-1.

The electron gun mount, Fig. II-4, consisted of a 5 1/4 in. long 3 in. O.D., 1/8 in. wall thickness brass tube. A 1/8 in. thick brass disk with a 5/8 in. hole through the center was soldered in the brass tube 1 1/4 in. from the end. The mount fit tightly into two LN_2 baffles, Fig. II-6, which were anchored to the LN_2 reservoir. The baffles provided both structural support and good thermal conductivity, allowing the mount to be cryopumped.

The Faraday cup, Fig. II-7, was constructed by soldering a 3/4 in. long solid copper cone into a 1 in. long, 1/2 in. O.D., copper tube. The Faraday cup fit in a teflon insulating sleeve which was supported by an LN_2 baffle. The current was monitored by a Keithly Model 610B electrometer.

REFERENCES FOR CHAPTER II

1. D.V. Horak, Ph.D. Thesis, University of California, Berkeley, LBL Report 14612 (1982).

2. J.R. Pierce, Theory and Design of Electron Beams, D. Van Nostrand Co., Inc., New York (1954), Chapter 10.

3. D.C. Hartman, Ph.D. Thesis, University of California, Berkeley, LBL Report 9819.

Table II-1

Typical Operating Conditions For The Electron Gun

Electron Gun Element	Voltage	Current
Filament	1.5v	3 amps
Filament Shield Filament Float	-60v to -180v	-
Lens 1	+200v	-
Lens 2	+300v	-
Final Focusing Stage	+50v	-
Faraday Cup	-	10^{-7} amps to 10^{-8} amps

Figure II-1. Interaction Chamber And Beam Source Pumping System

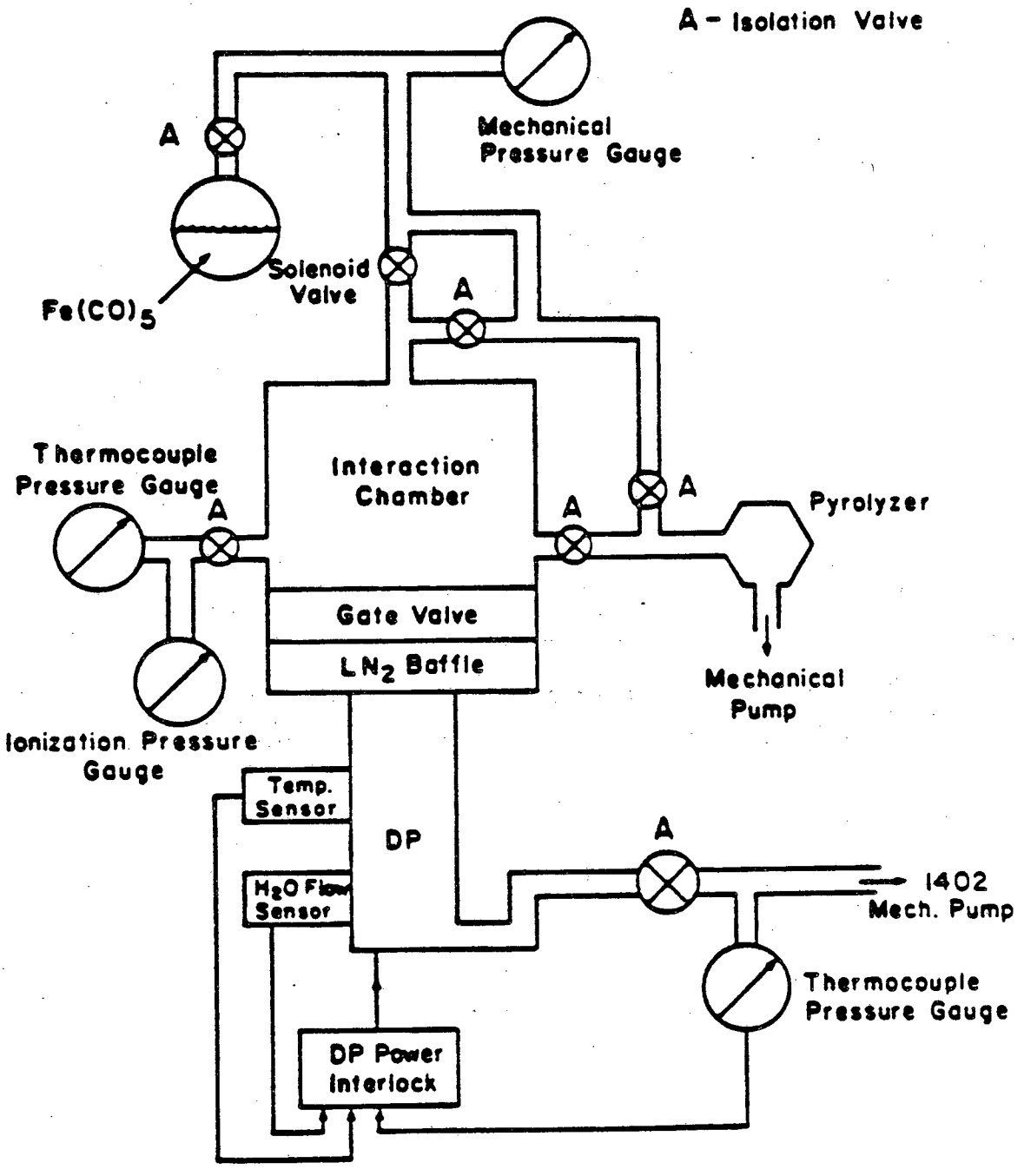

XBL 832-8105

Fig. II-1

Figure II-2. Interaction Chamber Cross-section

A. Electron Gun Mount Supports

B. Faraday Cup Support

C. Cryopump Baffle #1

D. Cryopump Baffle #2

E. Cryopump Baffle #3

F. Cryopump Baffle #4

G. Cryopump Body

H. Beam Nozzle

I. Electrical Feedthrough Flang

J. Cryopump Support Pillars

K. LN_2 Feed Tubes

L. Interaction Chamber Wall

M. Cryopump Slip-on Cover

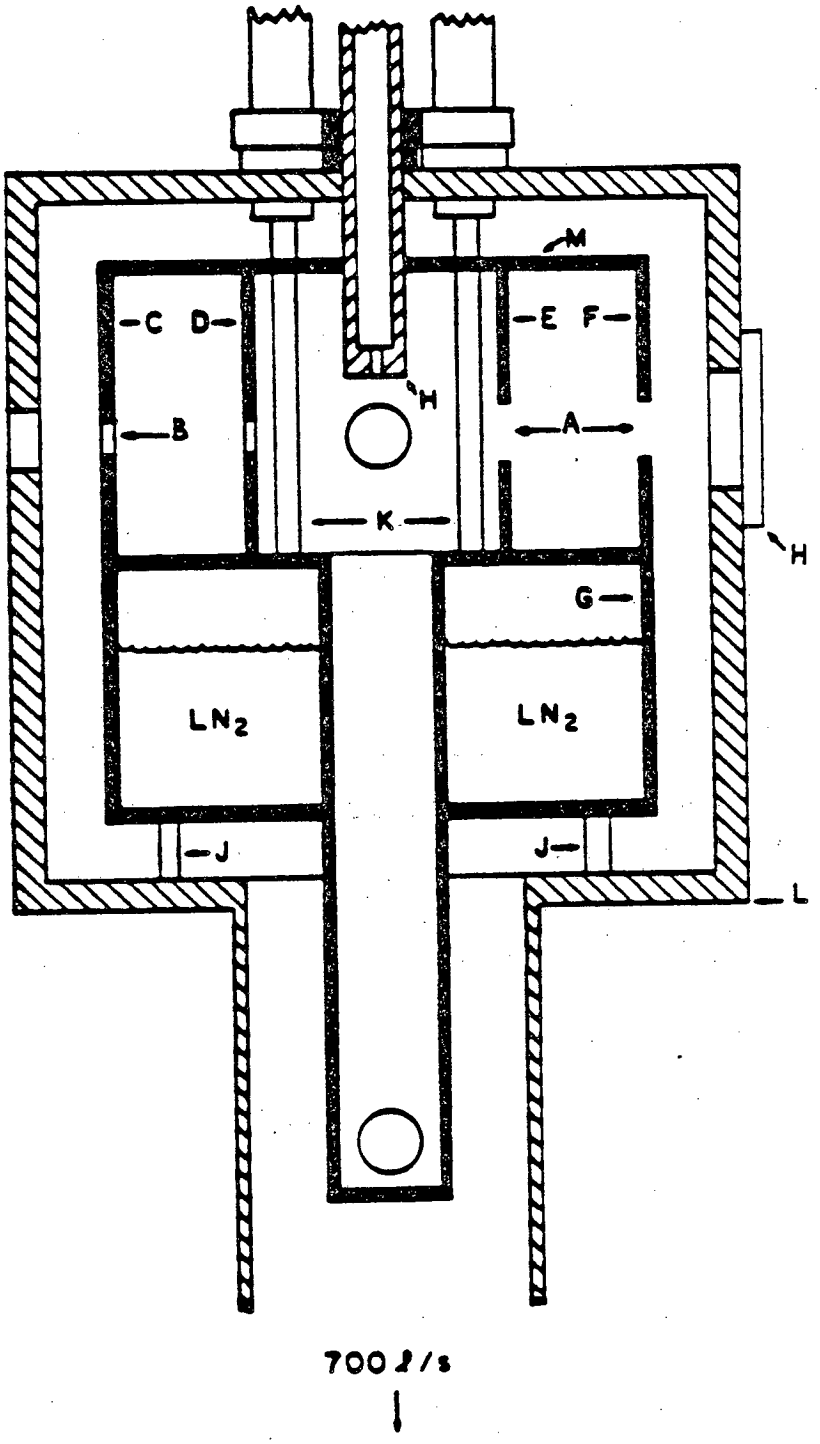

XBL 832-8104

Fig. II-2

Figure II-3. Electron Gun

A. Boron Nitride Filament Holder

B. Back Plate

C. Support For Electrcal Connections

D. Lens 1

E. Lens 2

F. Final Focusing Stage

G. Teflon Light Tight Ring

H. Front Plate

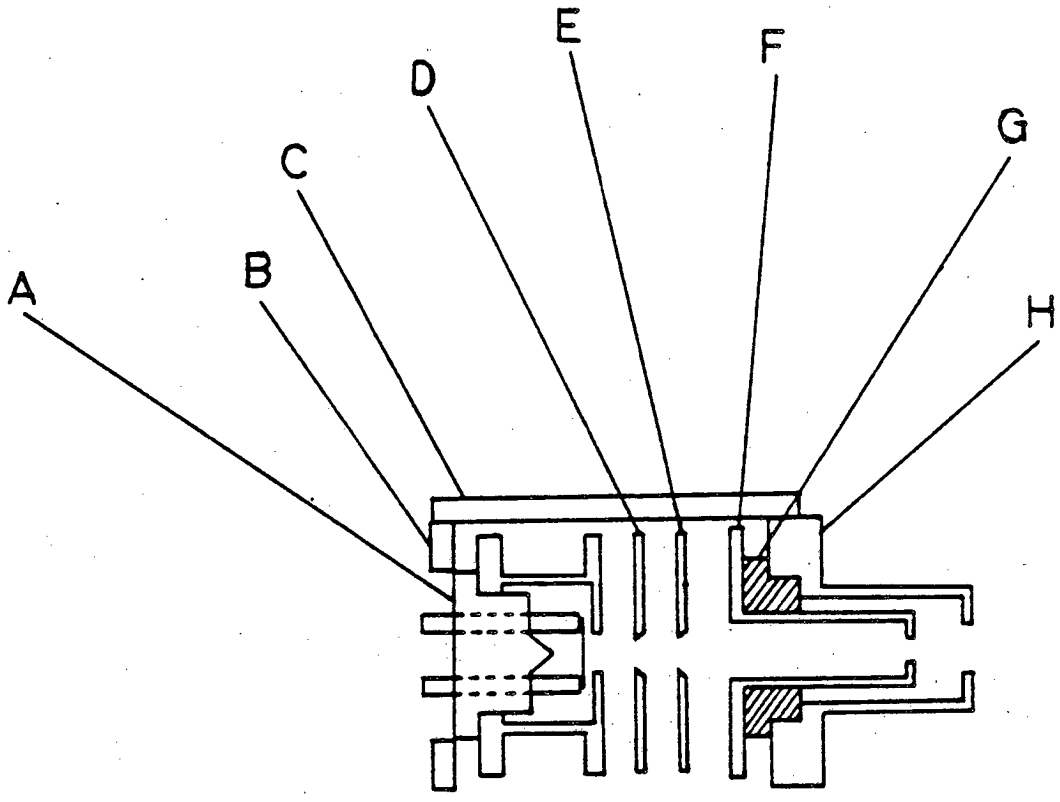

XBL 832-8103

Fig. II-3

Figure II-4. Block diagram of electron gun control electronics

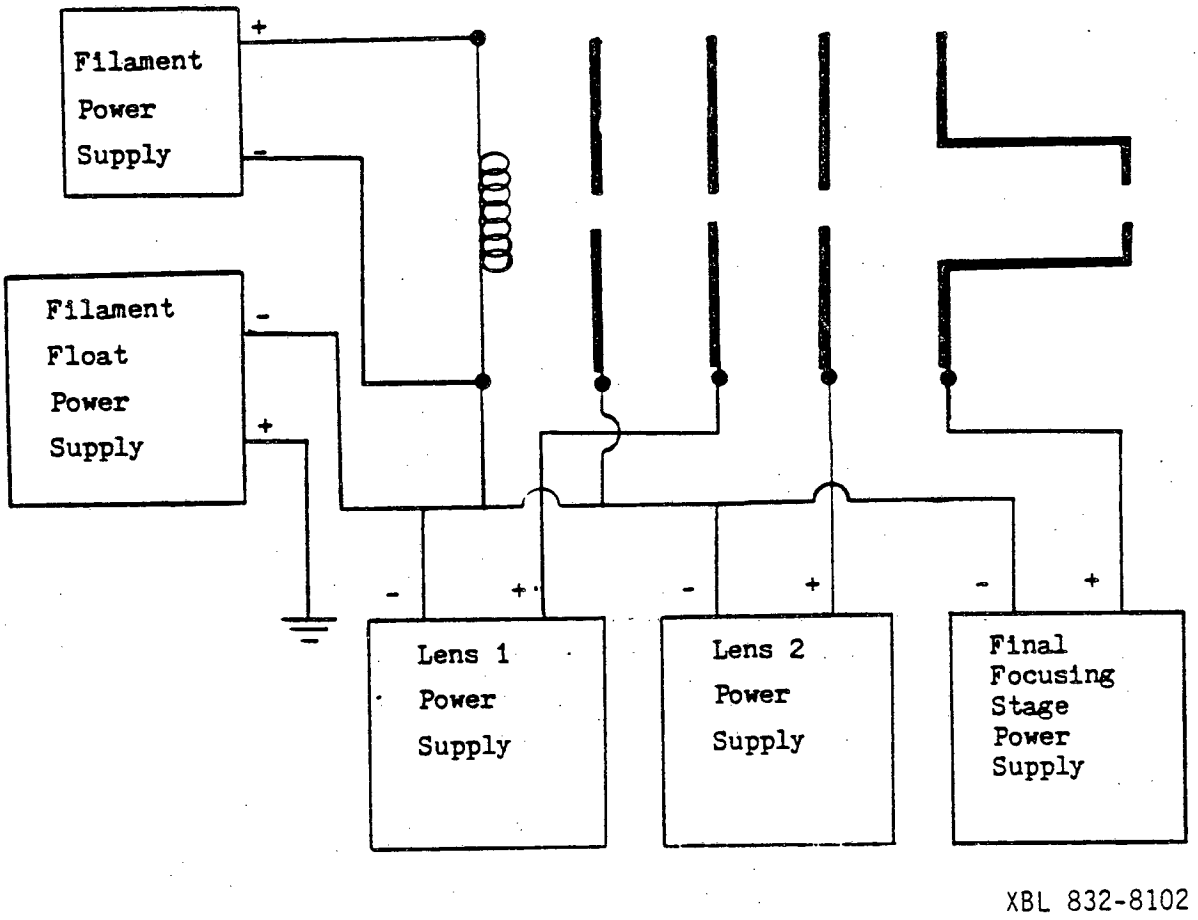
Filament
Power
Supply
+
-
Filament
Float
Power
Supply
-
+
-
+
-
+
-
+
Lens 1
Power
Supply
Lens 2
Power
Supply
Final
Focusing
Stage
Power
Supply
XBL 832-8102

Fig. II-4

Figure II-5. Electron Gun Mount

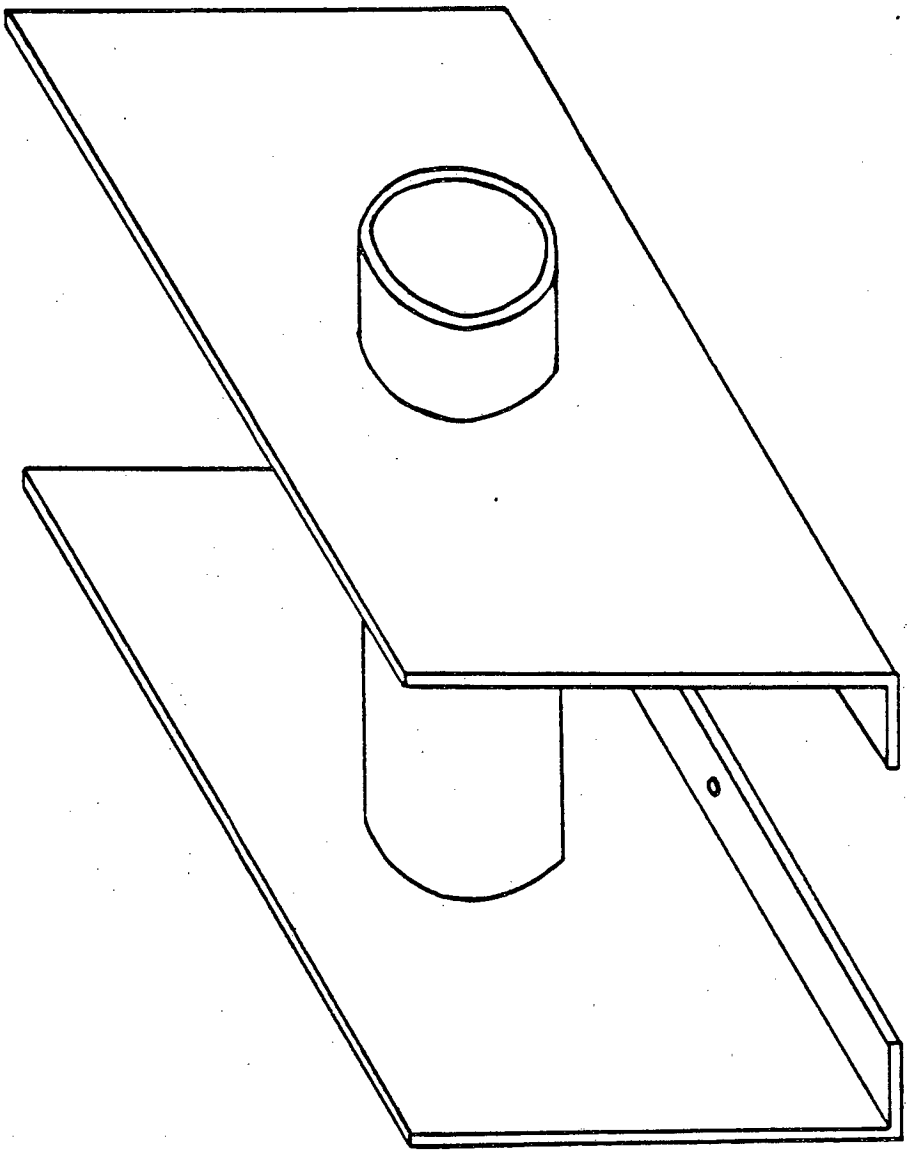

XBL 832-8101

Fig. II-5

Figure II-6. Cryopump Assembly

A. Cryopump Body

B. Cryopump Baffle #1

C. Cryopump Baffle #2

D. Cryopump Baffle #3

E. Cryopump Baffle #4

F. LN_2 Feed Tubes

G. Cryopump Slip-on Cover

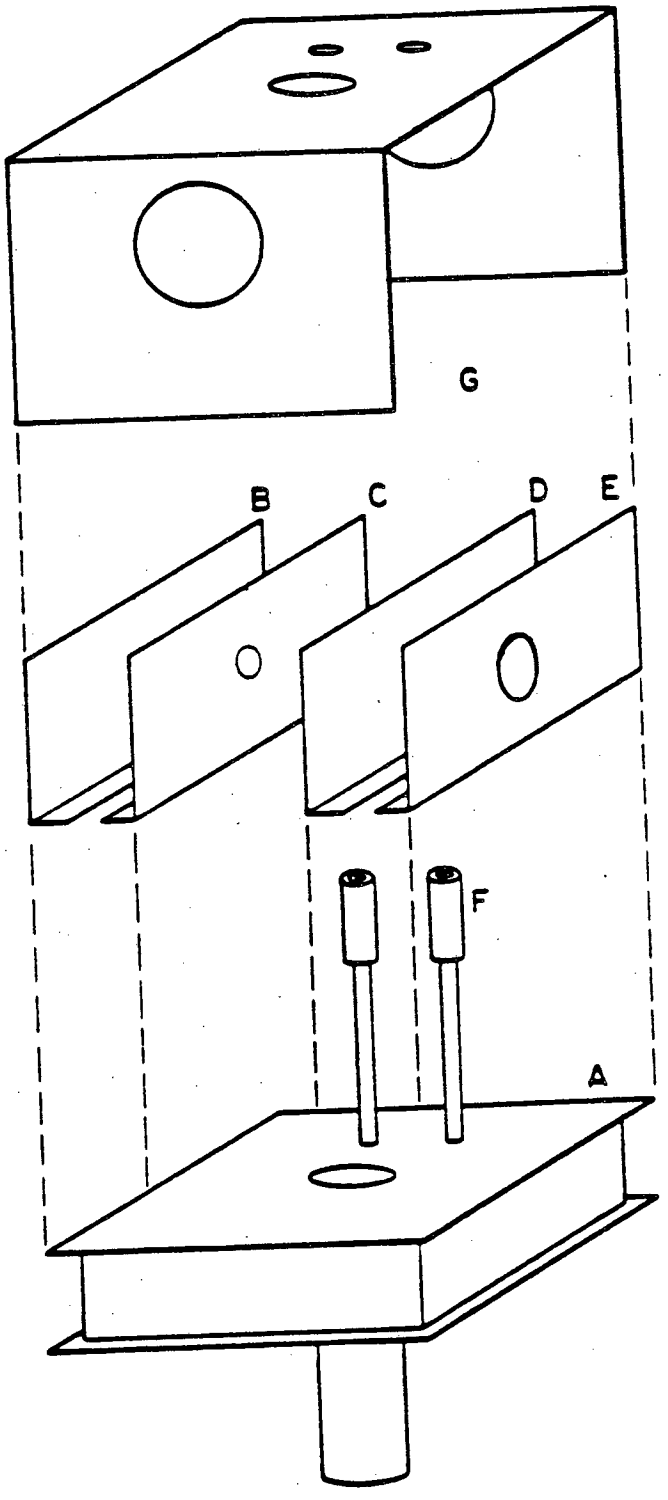

XBL 832-8099

Fig. II-6

Figure II-7. Faraday Cup

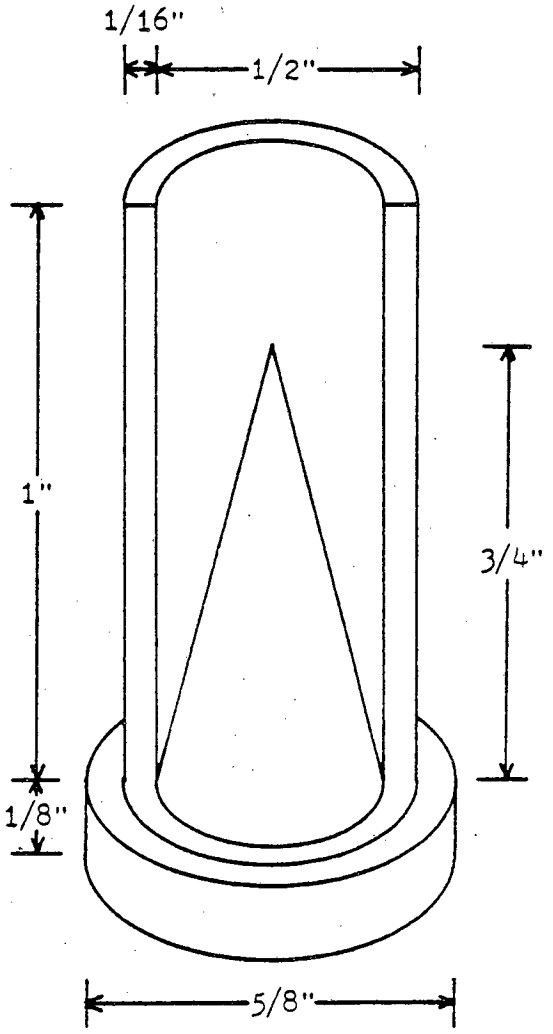

Faraday Cup

XBL 832-8100

Fig. II-7

Chapter III

EXPERIMENTAL PROCEDURES AND RESULTS

In order to determine the experimental characteristics of the fluorescence apparatus described in Chapter II, it was necessary to perform two experiments. First, by monitoring the total fluorescence as a function of time while monitoring the electron gun emission current, the stability of both the $Fe(CO)_5$ beam and the electron gun could be determined. Second, by monitoring the total fluorescence as a function of the electron beam energy, it could be determined at what energy the maximum fluorescence signal would be seen. This would be important to know since the dispersed fluorescence signal was expected to be small compared to the background.

A. Total Fluorescence vs. Time

1. Procedure

The diffusion pump was turned on four hours prior to the introduction of $Fe(CO)_5$. This insured an internal pressure of ca. 2×10^{-7} torr. Approximately two hours after the diffusion pump was turned on, the LN_2 reservoir was filled. This process normally took an hour and was then allowed to sit for an hour to allow all the baffles to be cooled to LN_2 temperature. During this time the sample reservoir was charged with approximately 300 grams of $Fe(CO)_5$. The $Fe(CO)_5$ was purified by freezing the sample in a dry ice/methanol bath while pumping on it for an hour with a mechanical pump. It then took about two hours for the sample to thaw and return to room temperature.

After the sample thawed, it was immersed in a water bath which main-

tained a constant temperature of 15°C. At this temperature the stagnation pressure was 25 torr, producing a flow rate of 8.2 gm/min. This flow rate allowed for about 30 minutes of beam time with a 1/4 in. I.D. nozzle.

The timing sequence is shown in Fig. III-1. It consisted of 20 seconds beam on, 20 seconds dead time and 20 seconds beam off for a total of 60 seconds per channel. The 20 seconds dead time allowed all the $Fe(CO)_5$ to leave the 20 cm. tube between the solenoid shut-off valve and the nozzle. This time was empirically determined to be sufficient by watching the photon counting rate meter drop from ca. 2×10^6 counts/sec to ca. 2×10^4 counts/sec about 12 seconds after the beam was turned off.

The electron beam energy was set at 100 v and the emission current at the onset of the experiment was 200 nanoamps. The emission current was monitored by a Keithly Model 610B electrometer. The photomultiplier measured about 10^4 counts/sec with the electron gun filament off and about 2×10^4 counts/sec with the filament on.

2. Results

Fig. III-2 is a plot of the emission current (in nanoamps) vs. time (1 min/channel). The drop in the emission current after about 25 minutes is due to iron poisoning the filament and was seen in all of the experiments performed on the apparatus. It was therefore necessary to monitor the emission current in all of the fluorescence experiments and adjust the fluorescence signal to compensate for emission current changes. Fig. III-3, is a plot of the total fluorescence vs. time. The fluorescence pattern closely follows the electron gun emission pattern of Fig. III-2. This indicates the limiting factor in the fluorescence was the electron

beam density and not the $Fe(CO)_5$ beam density. This in turn gives evidence that the experiment was linear with respect to emission current i.e., only one electron-molecule collision was involved in the process.

Fig. III-4 is a plot of the fluorescence background i.e., electron beam on, $Fe(CO)_5$ beam off. Fig. III-5 is the total fluorescence vs. time minus the background and adjusted for emission current. The stability of the beam in time (up to 60 minutes) as seen from this plot is quite good. The rather small fluctuations in the signal were probably due to fluctuations in the electron beam and not the $Fe(CO)_5$ beam. From this it was clear there was no long term changes in the beam density.

The experiment also allows calculation of a minimum quantum yield for fluorescence. At the start of the experiment the fluorescence signal was 1.5×10^6 counts/min. This is a minimum value since not all of the fluorescence could be collected due to the geometry of the collection system. The number of electrons absorbed was determined to be 3.7×10^{14} /min by measuring the difference in the emission current with the $Fe(CO)_5$ beam off and beam on. This is a maximum value since it only takes into account the electrons with trajectories that are within the solid angle of the Faraday cup. The fluorescence quantum yield is defined as the ratio:

$$Q.Y. = \frac{\text{Total \# of photons emitted}}{\text{Total \# of electrons absorbed X Acceptance Angle X Quantum Efficiency}} \qquad \text{(III-1)}$$

Thus, the minimum fluorescence quantum yield was calculated to be 2×10^{-4}. A further discussion of this and the fluorescence cross-section will be given in chapter IV.

B. Total Fluorescence vs. Electron Energy

1. Procedure

The procedure for this experiment was identical to that described in the previous section, except that the electron beam energy was varied from 60 v to 160 v at 20 v intervals. As described in chapter II, all the focusing grids and the filament power supplies were floated on the filament shield power supply which determined the energy of the electron beam. By floating the power supplies in this fashion, the electron beam could be varied without significant change in the focusing conditions. For each selected energy, data were accumulated for 3 channels. The emission current was monitored continuously.

2. Results

The results of this experiment are plotted in Fig. III-6. From this experiment it was clear that the maximum signal was at an electron energy of 100 v. The sharp decrease in fluorescence at 140 v and above indicates a rapid decrease in quantum yield. Also, it must be noted that at 60 v and below the emission current dropped off considerably i.e., by about a factor of 100. This indicates very poor focusing conditions existed below 60 v, which could account for the low fluorescence signal.

C. Dispersed Fluorescence

1. Procedure

The experimental procedure for the collection of the dispersed fluorescence was essentially the same as that for the undispersed fluorescence experiments previously described in this chapter, except for the following changes. The electron energy remained constant at 100 v. The fluor-

escence was dispersed by a 0.25 meter JA monochromator, Model 82-422, fitted with a 2360 grooves/mm grating blazed at 300 nm. The slits were 250 μm which resulted in a resolution of about 5 Å FWHM. The fluorescence was monitored with an EMI 9824B photomultiplier. The timing sequence used is shown in Fig. III-7. The sequence consisted of 4 scans. Each had 23 sec of accumulating data with the $Fe(CO)_5$ beam off, followed by 23 sec of accumulating data with the $Fe(CO)_5$ beam on, then followed by 14 sec of dead time to allow true beam off conditions before the next scan. The scan speed was 5 Å /min giving a rate of 20 Å/channel.

2. Results

Fig. III-8 is the fluorescence spectrum obtained by scanning the monochromator from 3500 Å to 4000 Å. The background in this region is shown in Fig. III-9. The fluorescence spectrum minus the background is shown in Fig. III-10. This spectrum corresponds to the fluorescence from the quintet states of atomic iron. A similar spectrum was observed by D.C. Hartman and J.S. Winn[3] using quenching of Ar^* and Ne^* metastables with $Fe(CO)_5$. This is also similar to the spectrum observed by D.V. Horak and J.S. Winn[1] using VUV photons.

Fig. III-11 shows the spectrum observed by scanning the monochromator from 4000 Å to 4500 Å. This corresponds to the region where one observes emission from the septet levels of atomic iron. Several scans were performed in this region with no emission lines visible. Horak and Winn[1] also observed no emission in this region. However, Hartman and Winn[2] did observe emission from the septet levels in this region.

REFERENCES FOR CHAPTER III

1. D.V. Horak, Ph.D. Thesis, University of California, Berkeley, LBL Report 14612 (1980).
2. D.C. Hartman, Ph.D. Thesis, University of California, Berkeley, LBL Report 9819 (1980).
3. D.C. Hartman, W.E. Hollingsworth, and J.S. Winn, J. Chem. Phys. 72, 833 (1980).

Figure III-1. Timing sequence used in nondispersed fluorescence data acquisition.

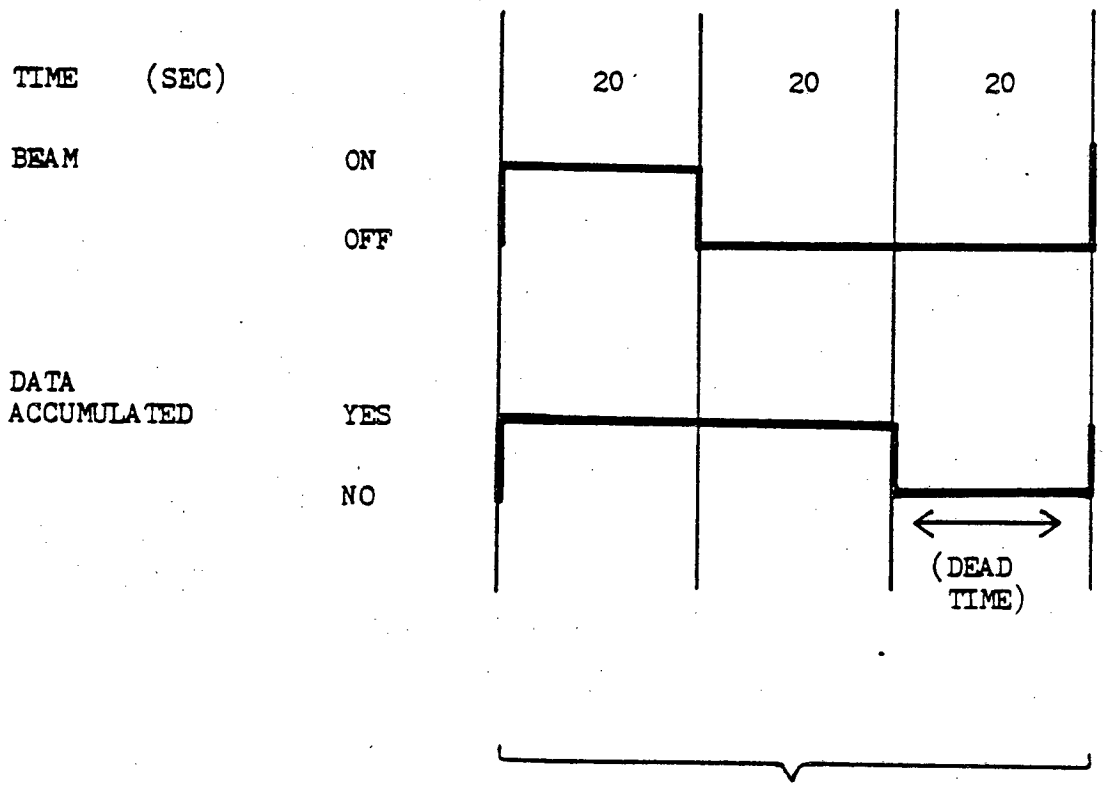

XBL 832-8098

Fig. III-1

Figure III-2. Electron gun emission current vs. time. Each channel is 60 sec.

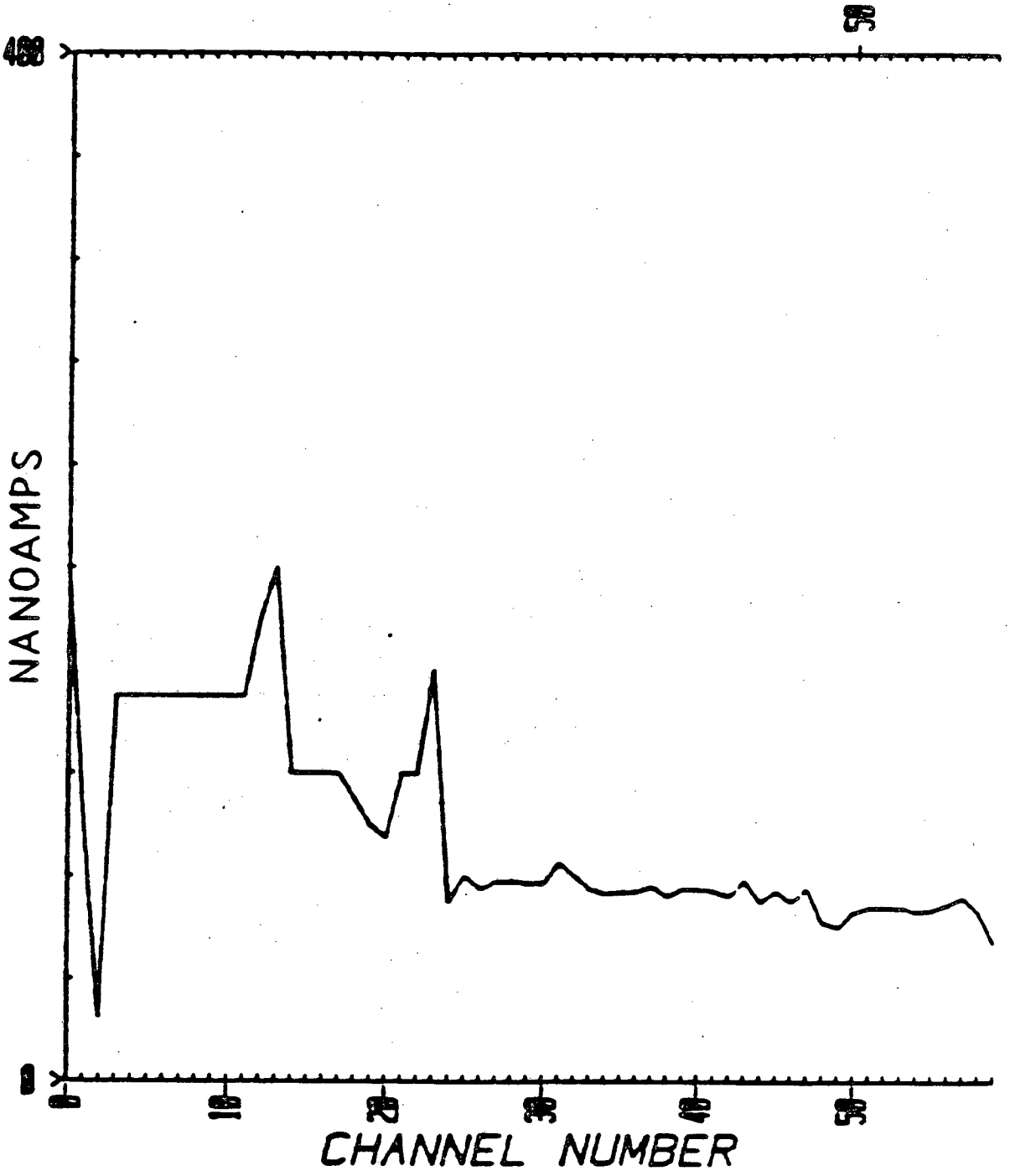

XBL 832-8097

Fig. III-2

Figure III-3. Total raw fluorescence vs. time. Each channel is 60 sec.

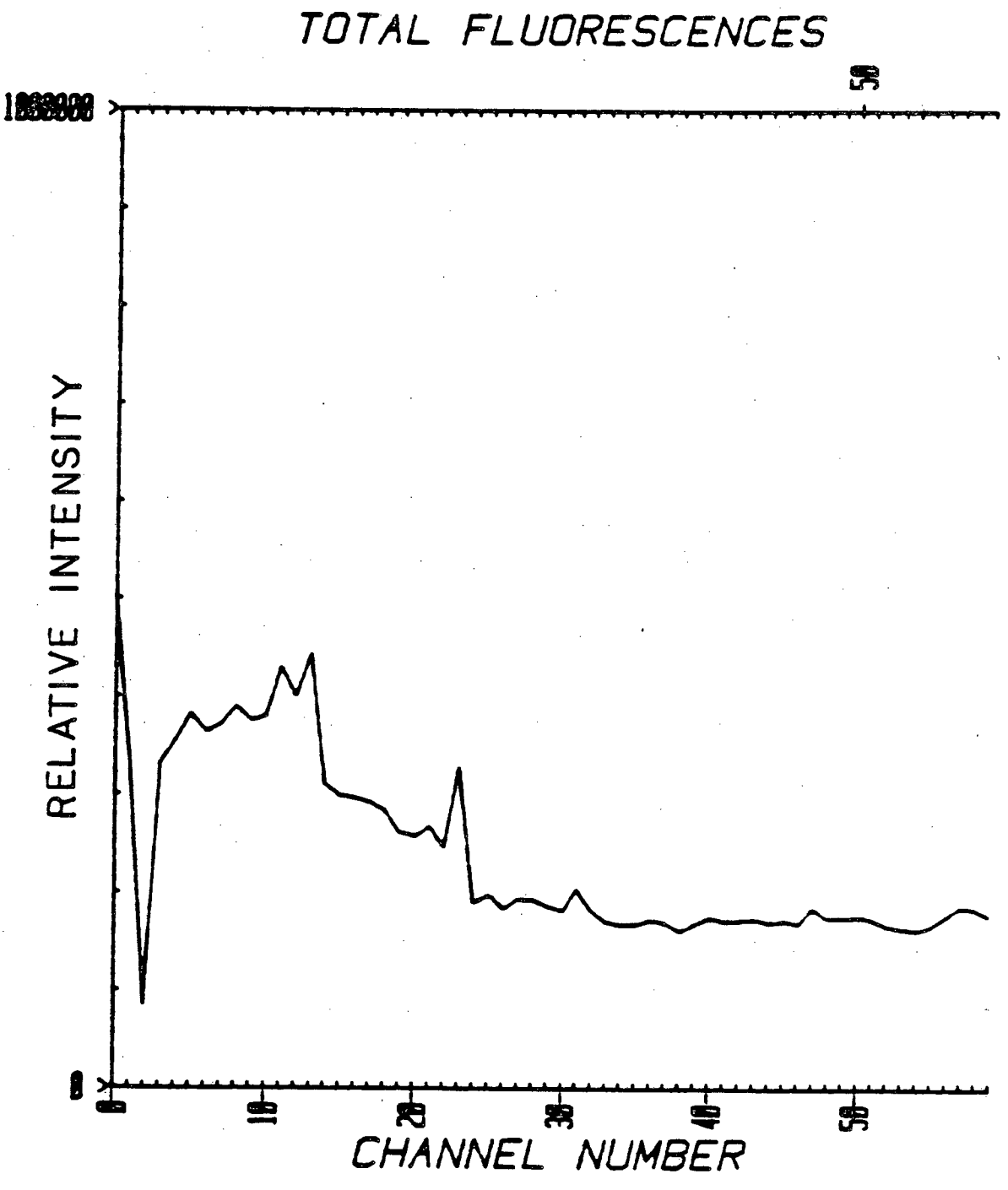

XBL 832-8096

Fig. III-3

Figure III-4. Background of total fluorescence vs. time.

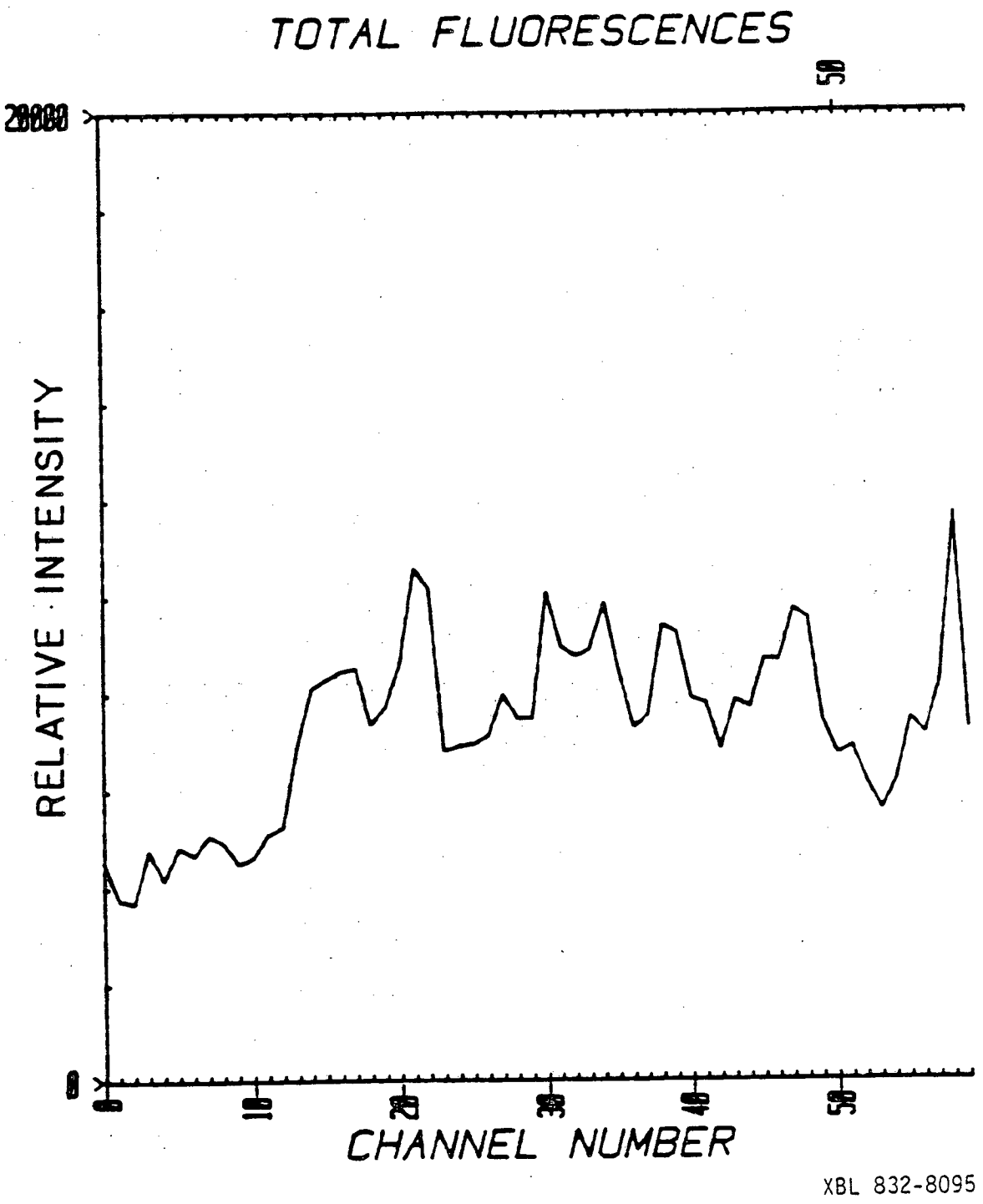
TOTAL FLUORESCENCES
RELATIVE INTENSITY
CHANNEL NUMBER
XBL 832-8095

Fig. III-4

Figure III-5. Total fluorescence vs. time minus background. (corrected for the emission current) Each channel is 60 sec.

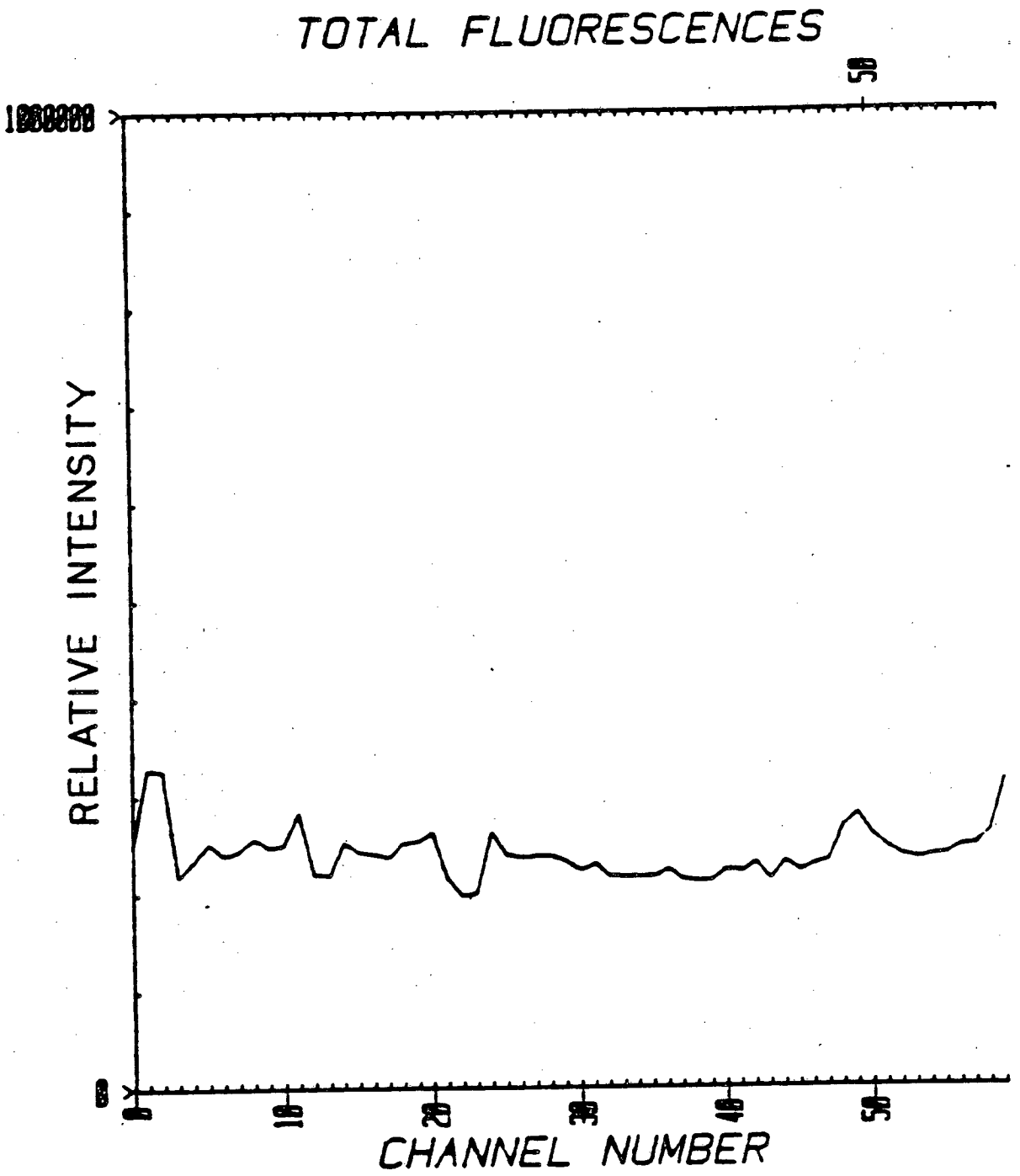
TOTAL FLUORESCENCES
RELATIVE INTENSITY
CHANNEL NUMBER
XBL 832-8094

Fig. III-5

Figure III-6. Total fluorescence vs. electron energy. (corrected for emission current)

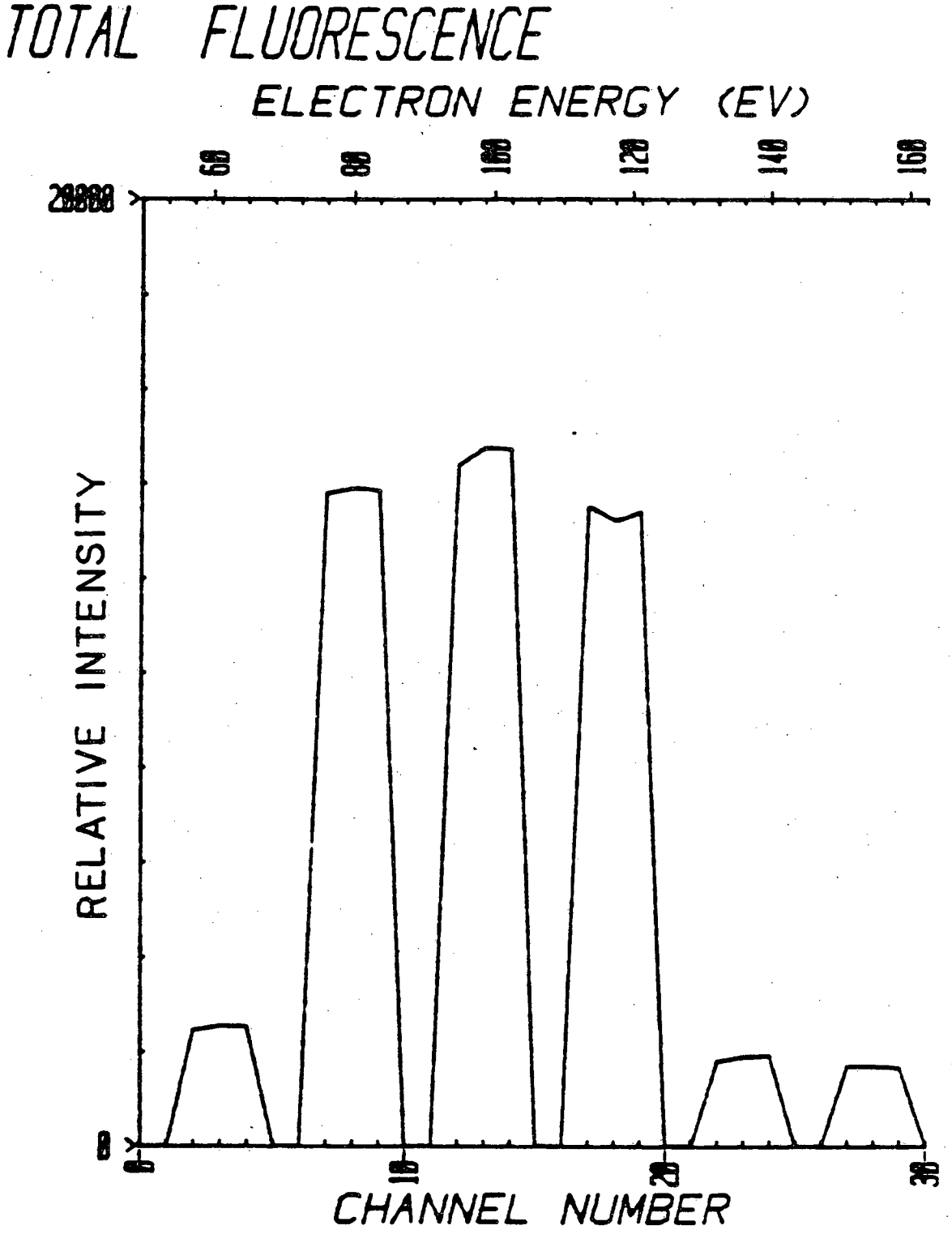

XBL 832-8093

Fig. III-6

Figure III-7. Timing sequence used in dispersed fluorescence data acquisition.

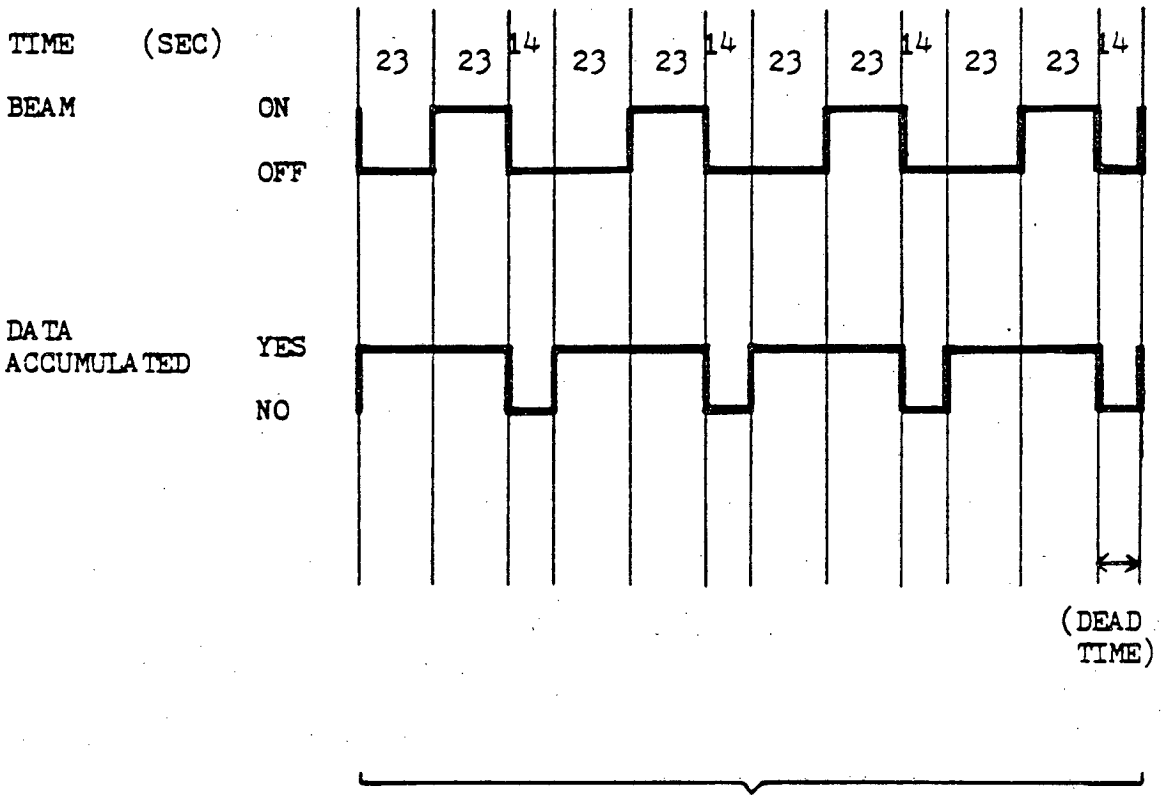
TIME (SEC)
BEAM
ON
OFF
DATA ACCUMULATED
YES
NO
23
23
14
23
23
14
23
23
14
23
23
14
(DEAD TIME)
1 CHANNEL, 4 MIN, 20 A
XBL 832-8092

Fig. III-7

Figure III-8. Dispersed iron fluorescence using electron impact. Electron energy set at 100 v.

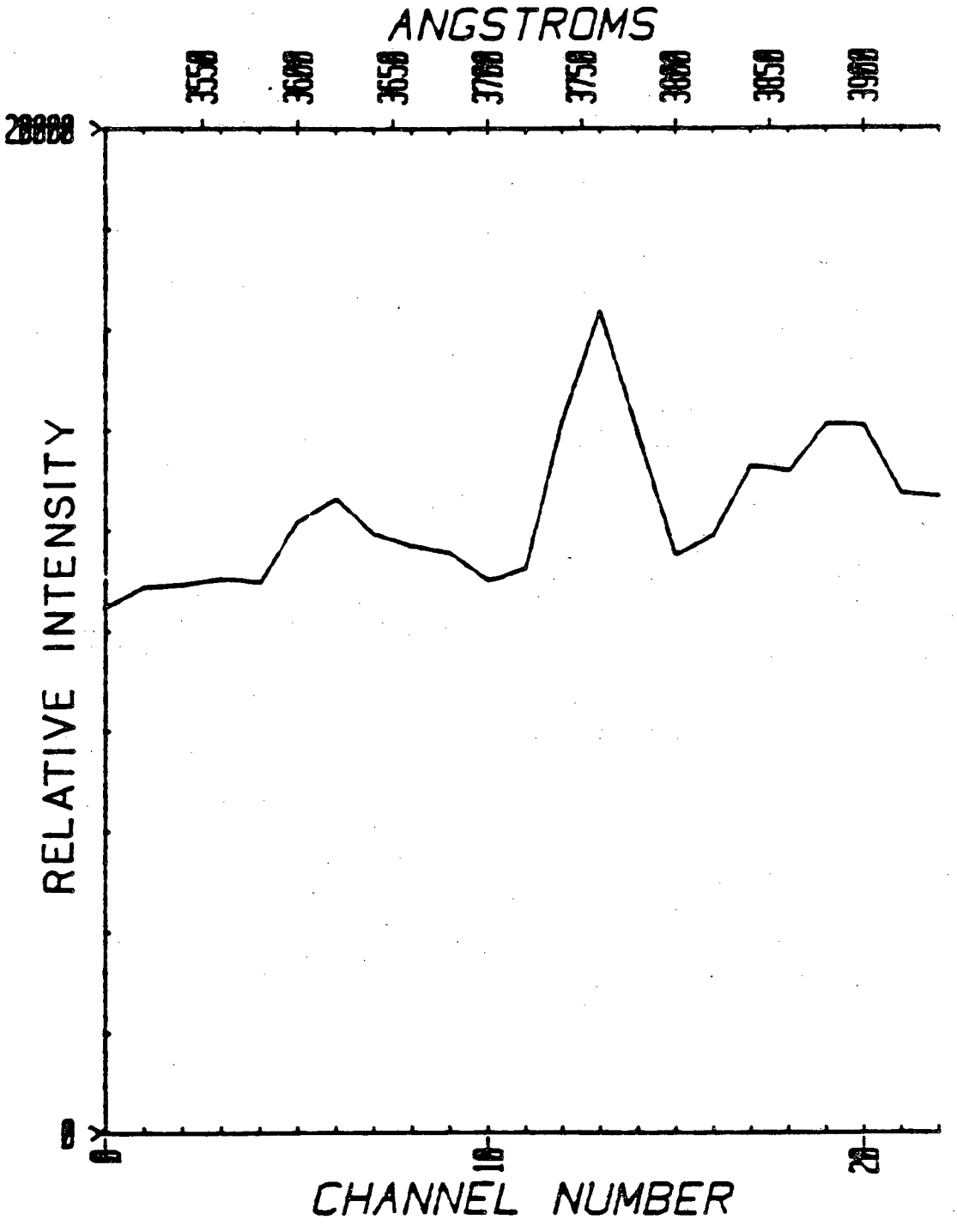

XBL 832-8091

Fig. III-8

Figure III-9. Background of dispersed fluorescence. Electron energy set at 100 v.

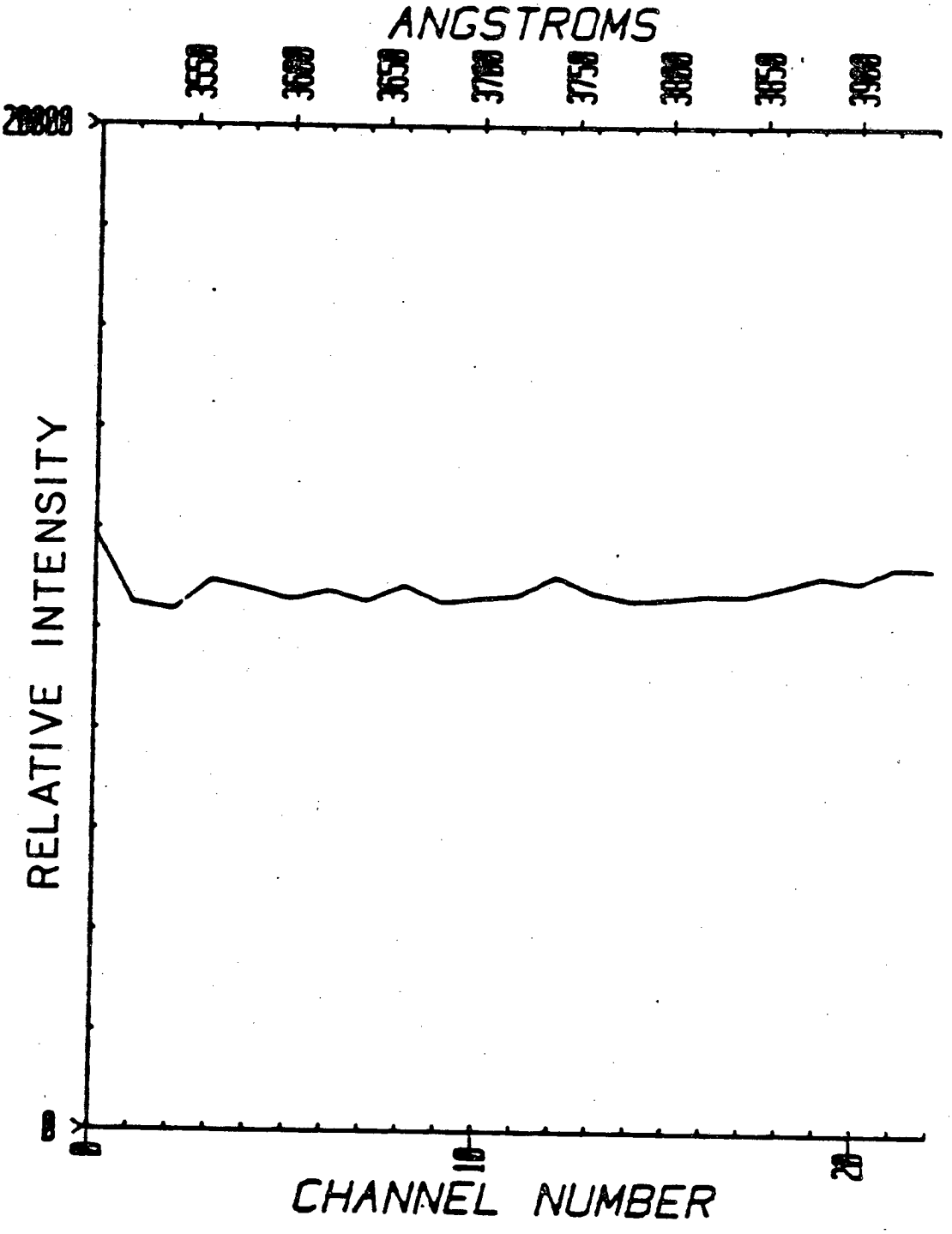

Fig. III-9

Figure III-10. Dispersed iron fluorescence minus background. Electron energy set at 100 v.

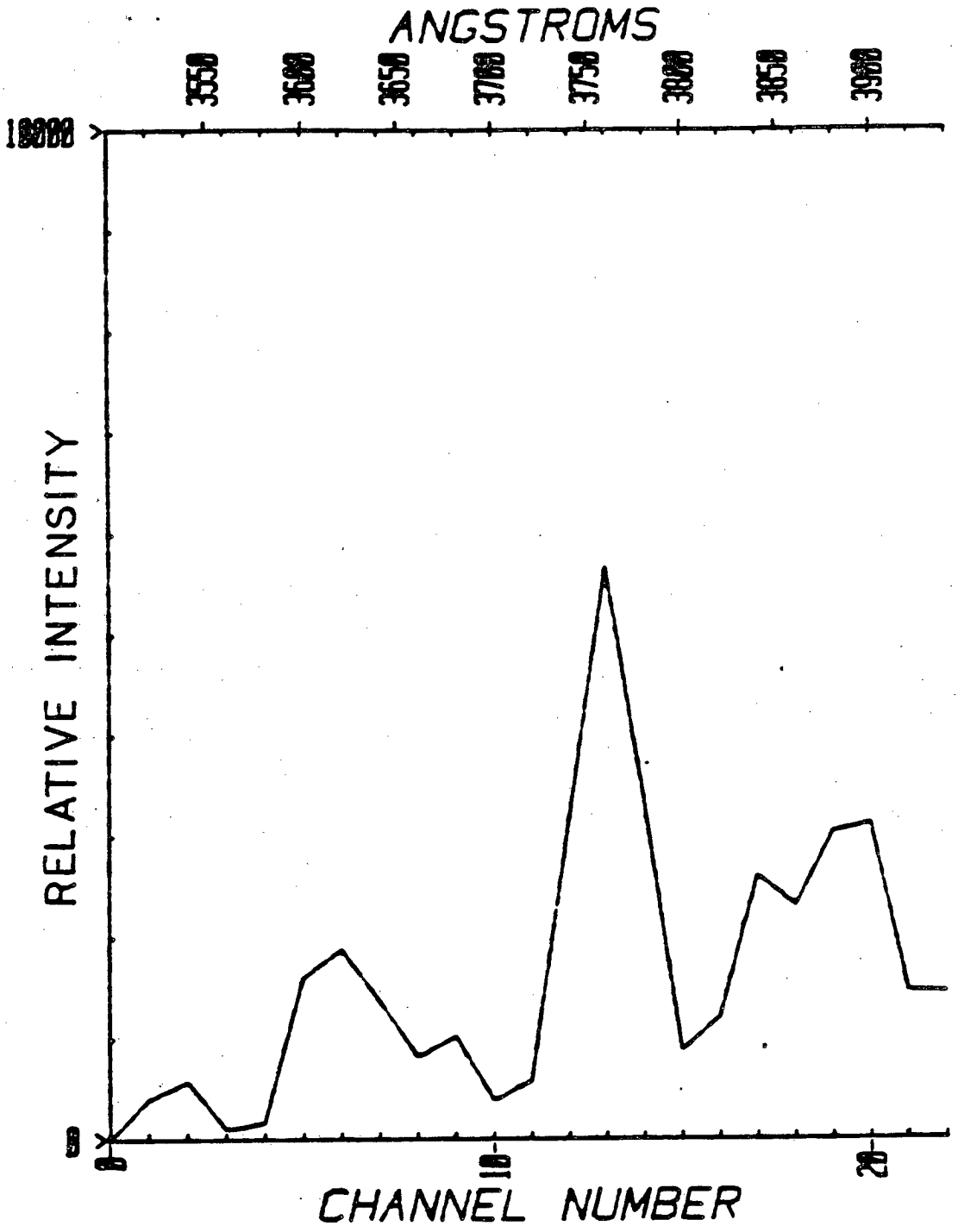

XBL 832-8089

Fig. III-10

Figure III-11. Dispersed iron fluorescence minus background. Electron energy set at 100 v.

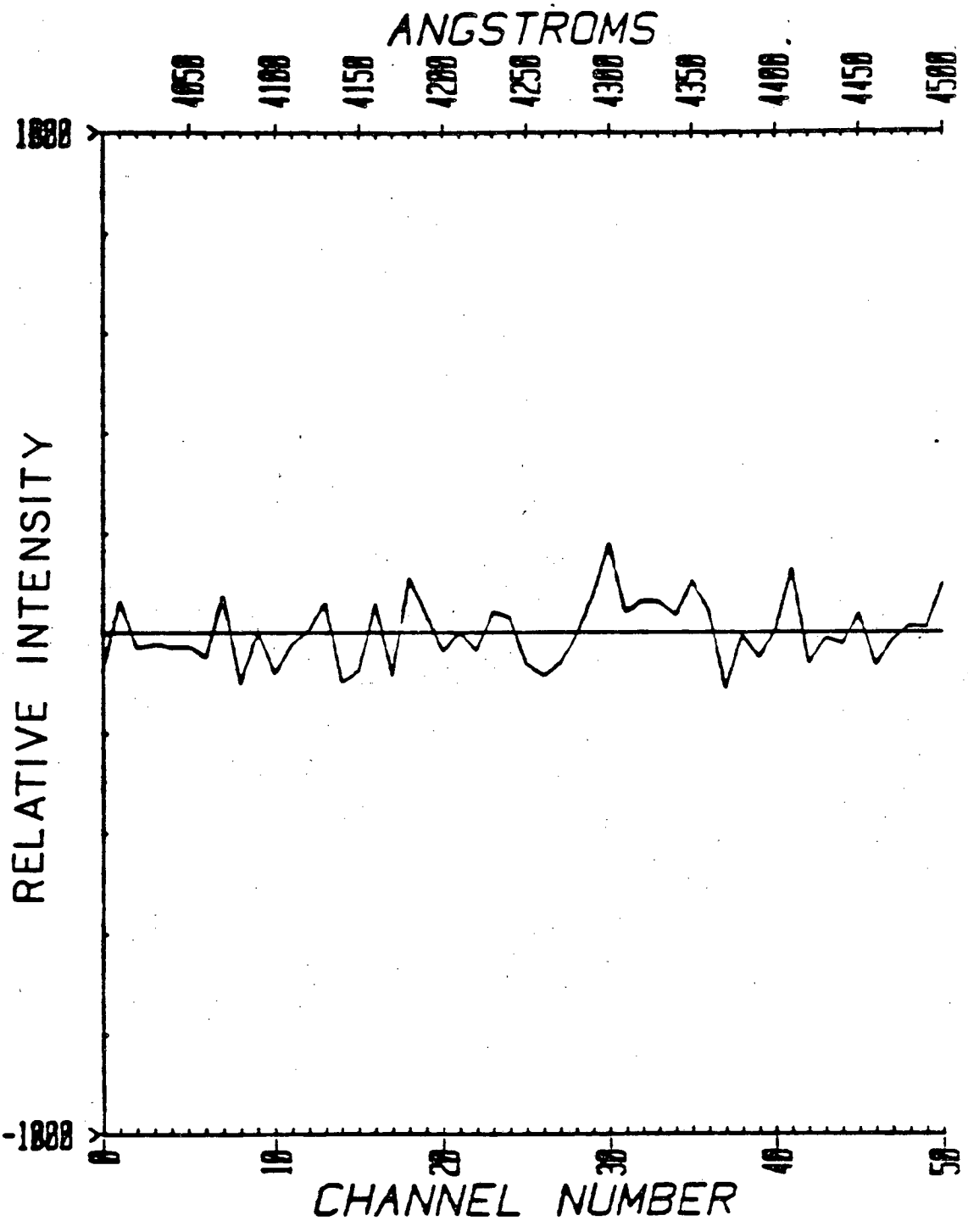

Fig. III-11

Chapter IV

DISCUSSION AND THEORY

In order to analyze the data obtained, it is necessary to determine the order of the $Fe(CO)_5$ electron interaction. As discussed in chapter III, the total fluorescence pattern closely followed the electron gun emission current. If the interaction between $Fe(CO)_5$ and electrons were not first order in electron flux, this would not be the case. If, for instance, the interaction was second order in electrons, the total fluorescence would decrease quadratically as the emission current decreased. The first order dependence on $Fe(CO)_5$ concentration was insured by operating the $Fe(CO)_5$ beam such that the molecules entering the interaction region were in the collisionless portion of the beam.

In chapter III, a total fluorescence quantum yield of 2×10^{-4} was determined. To obtain a fluorescence cross-section from this, it is necessary to know the beam density in the interaction region. A beam density of 0.047 torr or 1.5×10^{15} molec/cm^3 was determined by Horak[1]. This was accomplished by comparing an experimental absorption measurement with the known extinction value of $Fe(CO)_5$ and an empirical model for the density profile. His operating conditions were slightly different than those used in the experiments presented here. His reservoir temperature was 31.7°C, producing a vapor pressure of 40 torr, whereas, a reservoir temperature of 15°C was used here, producing a vapor pressure of 25 torr. From simple kinetic theory[2] the beam density, N_B, is related to the stagnation temperature and pressure by equation (IV-1).

$$N_B \propto \frac{P_s A}{T_s} \qquad \text{(IV-1)}$$

In equation (IV-1), A is the area of the effusion orifice. Using this relation and the beam density determined by Horak[1], a beam density of 9.9×10^{14} molec/cm^3 was obtained for the operating conditions used in the experiments presented here. It must be noted that this is an estimate of the beam density and the true beam density could vary from this value by 10%.

A total absorption cross-section 4.7 Å^2 $\pm$ 0.4 Å^2 was calculated using equation (IV-2).

$$\sigma_A = \frac{-\ln [I(1)/I(0)]}{N_B \, 1} \qquad \text{(IV-2)}$$

The ratio I(1)/I(0) was the fraction of the electron beam absorbed in the interaction region (ca. 10%) and the length of the interaction region, 1, was estimated at 5 cm. A total fluorescence cross-section of 9.4×10^{-4} Å^2 was calculated using equation (IV-3).

$$\sigma_{TF} = \sigma_A \times \text{Q.E.} \qquad \text{(IV-3)}$$

The large difference between σ_{TF} and σ_A will be discussed later in this chapter.

Because of the limited detection volume of the apparatus, a maximum lifetime limit for detection was imposed for long lived states. Only atoms that fluoresced before traveling through the 5 cm. detection region could be counted. The most probable Maxell-Boltzman velocity was determined by equation (IV-4)[2].

$$V_{mp} = \left[\frac{2\,RT}{M}\right]^{\frac{1}{2}} \qquad \text{(IV-4)}$$

In this equation, R is the gas constant in ergs $^oK^{-1}$ mole^{-1}, T is the temperature in ^oK, M is the molecular weight of the particle, and V_{mp} is in cm/sec. Because the limited degrees of freedom, statistical dissociation model[3] was expected to describe the process involved the value

of the mass used was196 gm/mole, the mass of $Fe(CO)_5$, and not 56 gm/mole, the mass of iron. (This model will be discussed later.) For this system $V_{mp} = 1.56 \times 10^4$ cm/sec. This allowed detection of only states with lifetimes shorter than 3.2×10^{-4} sec.

The limited degrees of freedom statistical dissociation model is explained in detail by Hartman[3], Hollingsworth[4] and Horak[1]. Briefly, this model suggests that during a collision, the electron (in this case) imparts an energy, E_e, to the $Fe(CO)_5$. This energy is internally randomized, and when the energy located in any iron-carbonyl bond is greater than its bond energy, a carbon monoxide molecule is liberated. The energy balance governing this process is:

$$E_u = E_e - E_d - E_m \qquad \text{(IV-5)}$$

where E_d is the energy required to rupture all iron-carbonyls, E_m is the energy required for electronic excitation of the iron atom, and E_u is the excess energy. This excess energy must be partitioned into the electronic, vibrational, rotational and translational modes of the carbonyls. It is then postulated that the relative production rate of an excited iron state at an energy E_m above the ground state is proportional to the total density of states $\rho(E_u)$ for all the allowed degrees of freedom available in the collision complex.

$$M^* \propto \rho(E_u) \qquad \text{(IV-6)}$$

The density of states, $\rho(E_u)$, can be obtained by taking the inverse Laplace transform of the total partition function for all the active degrees of freedom.

$$\rho(E_u) = \cdot L^{-1}\left\{q_{total}\right\} \qquad \text{(IV-7)}$$

The total partition function can be viewed as the product of the component partition functions if they are seperable i.e., the motion of the

components are independent. For the system discussed here, this gives a total partition function:

$$q_{total} = q_t\, q_r\, q_v\, q_e \qquad \text{(IV-7)}$$

where q_t is the translational partition function for each CO, q_r is the rotational partition function for each CO, q_v is the vibrational partition function for each CO and q_e is the electronic partition function for each CO. For an unlimited degrees of freedom statistical model, all these components of motion would be used to calculate the total partition function. However, it has been found [1,3] that by limiting the degrees of freedom to only translation and vibration, the total partition function more closely predicts the dissociation rate for $Fe(CO)_5$ - VUV photon and $Fe(CO)_5$ - metastable rare gas. Also, the translational partition function is limited to a one dimensional translator. What this suggests is that the dissociation process is virtually simultaneous i.e., fast enough that rearrangement is not possible.

Horak[1] and Hartman[3] applied this model to the dispersed fluorescence spectrum they obtained from $Fe(CO)_5$ - VUV and $Fe(CO)_5$ - metastable rare gas collision, respectively. Comparison of the dispersed fluorescence from electron impact, Fig. (IV-1), and the dispersed fluorescence from VUV and metastable excitation, Fig. (IV-2) and Fig. (IV-3), shows all these processes to be similar. This indicates the limited degree of freedom model could be applied to electron impact dissociation of $Fe(CO)_5$.

Thus far, the possibility of electron impact ionization of $Fe(CO)_5$ has not been discussed. This is an important and probably the dominant process involved in these experiments. This could explain the large difference between the absorption cross-section and the fluorescence cross-section discussed previously. Electron impact has been used as an effi-

cient means of producing ions in mass spectrometric studies[4,5] for a long time. Winters and Kiser[5] have shown that electron impact of $Fe(CO)_5$ produces $Fe(CO)_5^+$, which then dissociates by successive removal of neutral CO groups to form $Fe(CO)_{5-n}^+$ where n=0,1,2,3,4,5. This is in direct contrast to the limited degrees of freedom model discussed previously.

The evidence presented here indicate the two processes involve different collisional complexes. In the case of ionization, this complex is short lived, similar to electron stripping. Before complete randomization of the energy can occur, ionization and dissociation take place. In the case of neutral dissociation fluorescence, randomization of the energy does occur before the dissociation process. However, this process is completed on a time scale faster than a rotational period of the $Fe(CO)_5$ in order for the CO groups to leave without experiencing any rearrangement. This would be similar to an impulsive dissociation mechanism.

A summary of the absorption cross-sections σ_A and the total fluorescence cross-sections for chemiluminescence VUV photolysis and electron impact is shown in Table IV-1. In the case of both VUV photolysis and electron impact there is a large difference between σ_A and σ_{TF}. Although the ionization cross-section was not measured in the present work, it is expected to be larger than the total fluorescence cross-section, σ_I, as reported for photolysis.[1] Also, similar to photolysis, largest competing cross-section is believed to correspond to the production of ground and low living nonradiative state of iron, σ_{NR}. The postulated dissociation model is:

$$Fe(CO)_5 + e^- \xrightarrow{k_A} \underbrace{Fe(CO)_5^* + e^-}_{Fe^* \text{ (fluorescing states) } +5CO} \rightarrow Fe^* \text{ (ground and +5CO nonfluorescing existed states)}$$

$$Fe^+ + 5CO$$

It must be noted that production of negative ions is unlikely at these energies.[6]

To fully understand this discrepancy, it would be helpful to measure the rate of successive removal of CO groups from $Fe(CO)_5^+$. This could be measured by forming $Fe(CO)_5^+$ in an ion trap and sampling the trap at various times. Another experiment that would be useful would be to look at a single iron line while at the same time monitoring the ion production, thus observing the ion-neutral branching ratio as a function of electron energy.

REFERENCES FOR CHAPTER IV

1. D.V. Horak, Ph.D. Thesis, University of California, Berkeley, LBL Report 14612 (1982).
2. J.R. Pierce, Theory and Design of Electron Beams, D. Van Nostrand Co., Inc., New York (1954), Chapter 10.
3. D.C. Hartman, Ph.D. Thesis, University of California, Berkeley, LBL Report 9819 (1980).
4. W.E. Hollingsworth, Ph.D. Thesis, University of California, Berkeley, LBL Report 14917 (1982).
5. R.E. Winters and R.W. Kiser, Inorg. Chem. 3, 699 (1964).

Table IV-1

Experiment	Electron Impact	Rare Gas ** Metastable Quenching	VUV Photolysis
Absorption * cross-section σ_A	4.7 ± 0.4	4	1.3 ± 0.2
Total Fluorescence cross-section σ_{TF}	$9.4 \pm 0.8 \times 10^{-4}$	1	$1.7 \pm 0.3 \times 10^{-4}$
Non-Fluorescence* cross-section σ_{NF}	4.7 ± 0.4	3	1.3 ± 0.2

* Cross-sections are given in Å^2

** No estimation of error was given

Figure IV-1. Electron impact dispersed fluorescence. Lines show relative intensities of iron emission reported by Hellner et al.[6]

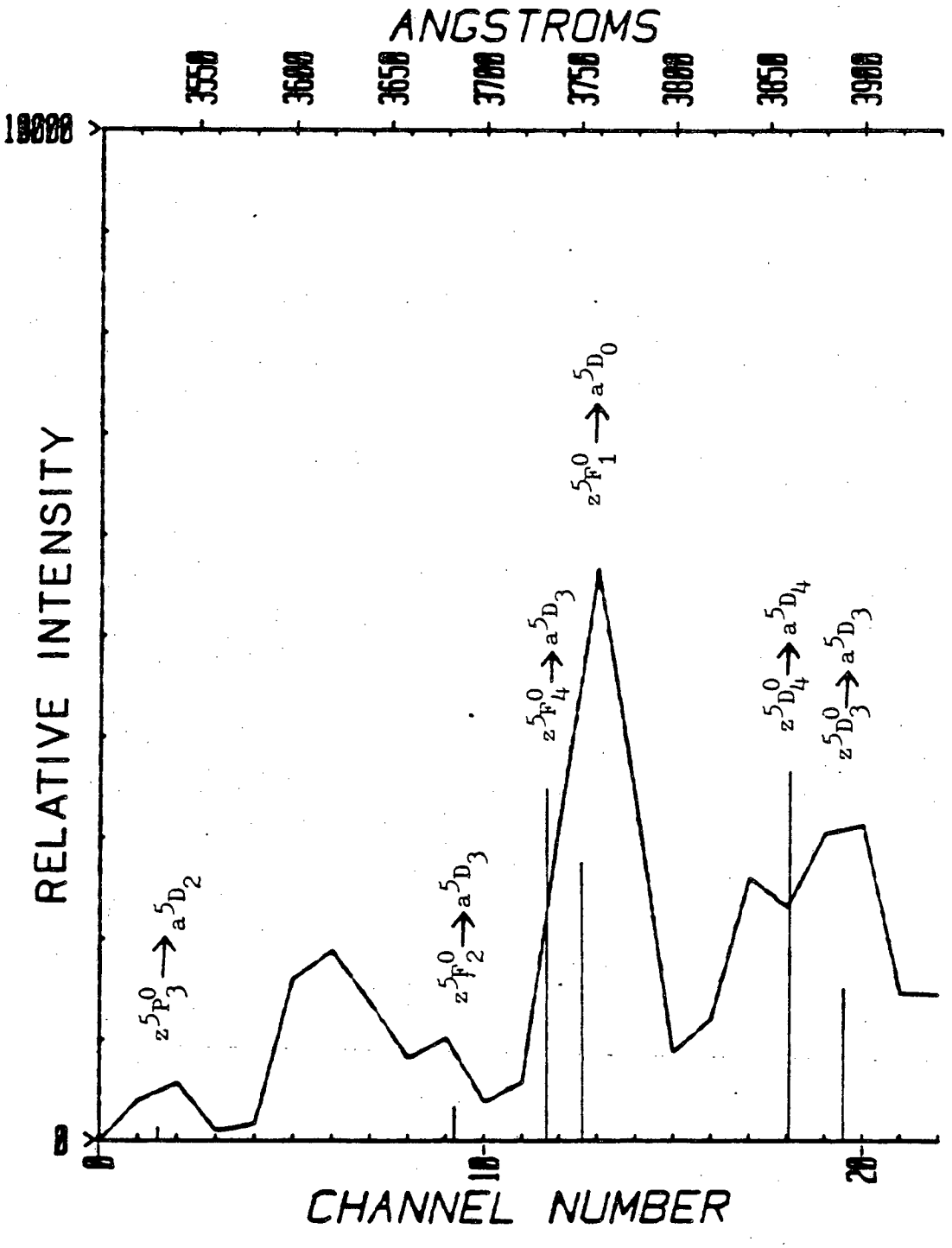

XBL 832-8087

Fig. IV-1

Figure IV-2. VUV induced iron fluorescence

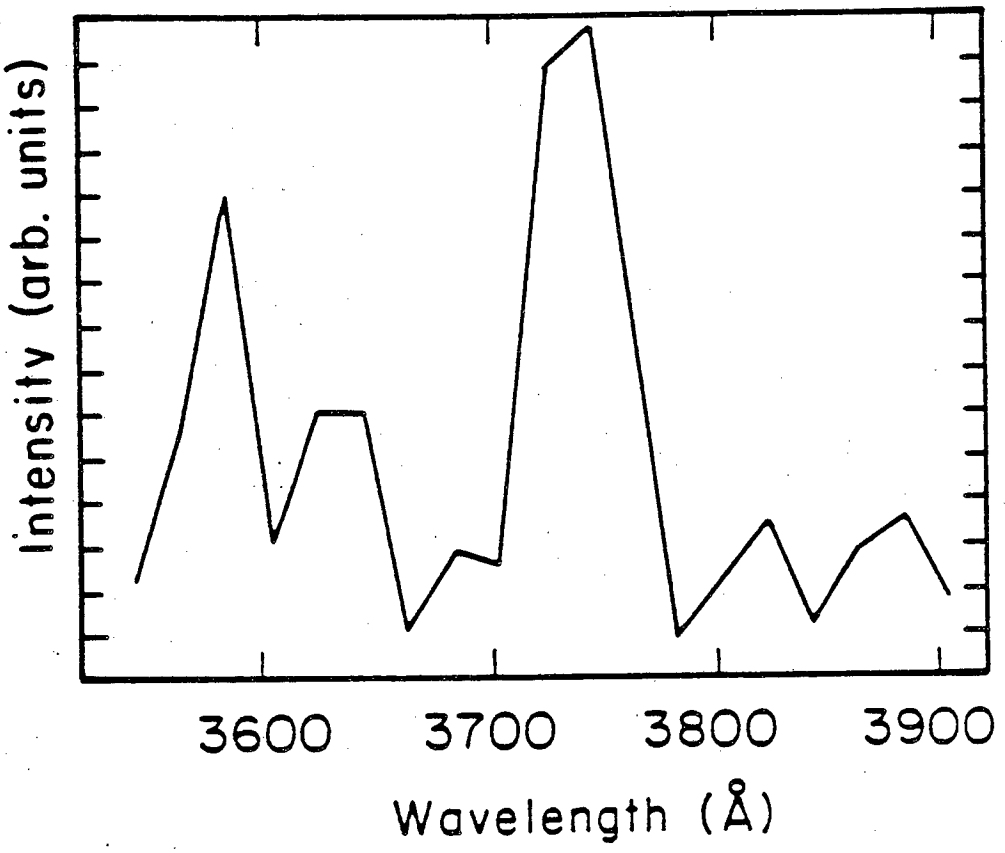

XBL 832-8086

Fig. IV-2

Figure IV-3. Neon metastable induced iron fluorescence

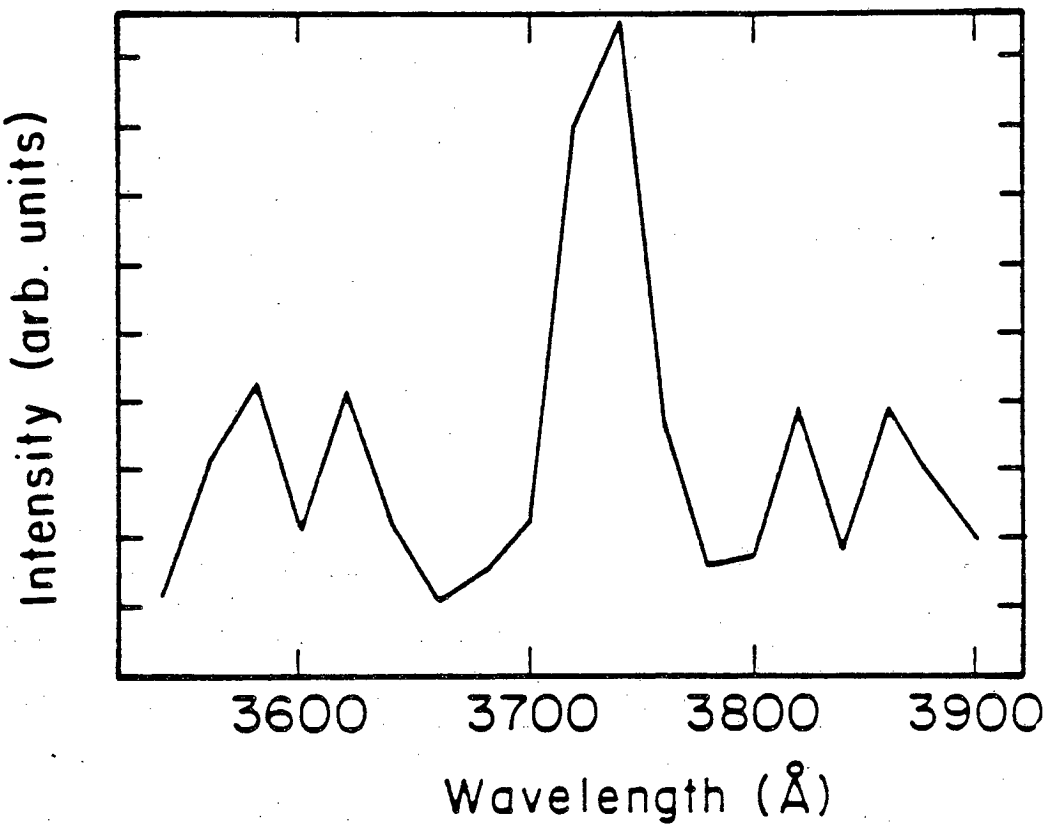

XBL 832-8085

Fig. IV-3

Chapter V

FORMATION OF THIN IRON FILMS

The formation of thin metal films by dissociation of organometalics has long been observed.[1,2,3] Nickel films formed by the thermal decomposition of nickel tetracarbonyl have been shown to be active hydrogenation catalysts.[1] Derouane et al.[2] studied the formation of iron films using both photo and thermal decomposition of $Fe(CO)_5$. This study showed that photodecomposition results in smaller particle size. This is the result of a difference in the interaction between the intermediates and the surface.

With the development of microelectronics it has become increasingly more important to study the formation of thin films with greater spatial resolution using metal and semiconductor material. High spatial resolution may not be possible using either thermal or photodecomposition since in both cases the decomposition of the precursor could be some distance from the surface where the film is to be formed. However, if electrons ejected from the surface by UV photons could be used to form the dissociated intermediates, the spatial resolution would be a function of the absorption cross-section and the pressure.

Three experiments have been performed to determine the plausibility of the above process. Each of these experiments will be discussed in the following sections.

A. Photoemission Current vs. Film Growth

Fig. V-1 shows a schematic diagram of the experimental apparatus. The vacuum chamber consisted of a 6 in. I.D. Pyrex tee. The chamber was

evacuated by a Welch 1402 mechanical pump which could produce a vacuum of ca. 10 microns. $Fe(CO)_5$ was introduced through a 1/4 in. O.D. stainless steel tube. A soda glass target was mounted to a support rod connected to the top flange. A coaxial insulated wire was clamped to the soda glass at one end. The other end was connected to a Keithly Model 610B electrometer. A 1000 watt Hg/Xe high pressure lamp was focused through a quartz window onto the target glass. The area of the target glass was approximately 4 cm^2.

Because the work function of iron is much lower than that of soda glass, the rate of film growth could be measured by monitoring the increase in the photoemission current. At the start of the experiment the photoemission current was approximately 10^{-12} amps or 0.25×10^{-12} amps/cm^2 assuming the target was uniformly illuminated. This compares very well with the results of Rohatgi.[4] The photoemission current increased to about 10^{-10} amps or 0.25×10^{-10} amps/cm^2 approximately 10 minutes after $Fe(CO)_5$ was introduced. If at any point the light was blocked, the photoemission current would drop to below 10^{-13} amps, the detection limit of the electrometer.

Monitoring the photoemission current was hampered by rather large fluctuations in the signal. This was partly because of the instability of the Hg/Xe power supply. Because of these fluctuations no expression for the rate of film formation could be determined. Also, there was no evidence indicating whether the films were formed through dissociation by electron impact or through photodissociation. However, the results do indicate that photoemission does occur under these conditions and that films did grow on the target surface.

B. A Comparison of Soda Glass and Quartz as Surface Substrates

Fig. V-2 shows a schematic diagram of the experimental apparatus. The cell, Fig. V-3, consisted of a brass body and two quartz windows. The cell held two surfaces, one quartz and one soda glass. The relative rates of film growth was measured by monitoring the optical density of both substrates with photodiodes. The photodiodes were connected to a differential amplifier which was adjusted to zero at the start of the experiments.

In each of the experiments the light passing through the soda glass was attenuated faster than the light passing through the quartz. However, a thin film did eventually appear on the quartz substrate. This experiment was plagued with one major problem. Vibrations from the mechanical pump would misalign the photodiodes quite rapidly (about 2-5 min). All efforts at trying to decouple this vibration failed. Because of this, no quantitative information was obtained. However, the results did show that the soda glass was a better substrate for film growth. This should be compared to what Becuchamp[5] observed with glass and silver substrates. Their results showed films grow on silver substrates 45 times faster than on glass. The results discussed are compatible with an electron dissociative attachment from photoejected electrons model. However, this does preclude the possibility that the films are formed through photodissociation and the difference in the rates of film formation are due entirely to surface effects.

C. Kinetics Study

The apparatus was modified with the addition of a MKS Baratron 0.0001

to 0.1 torr capacitance manometer and several isolation valves, Fig. V-4. This allowed continuous monitoring of the total pressure inside the sample cell. A soda glass substrate was used as a target. For each iron atom that was absorbed on the surface, five CO groups were left. Therefore, by monitoring the pressure a rate expression could be determined for the dissociation of $Fe(CO)_5$.

Fig. V-5 is a typical plot of the increase in pressure vs. time. The starting pressure of these experiments ranged from 0.05 torr to 0.001 torr. The change in starting pressure had no effect over the general shape of these curves. Assuming both photodissociation and electron dissociative attachment occured, the rate of iron deposition would be described by equation (V-1).

$$\frac{d[Fe_s]}{dt} = \varphi[Fe(CO)_5]_t\{k_p + k_e[Fe_s]_t\} \qquad (V\text{-}1)$$

In equation (V-1), $[Fe_s]_t$ is the amount of iron deposited at time t, $[Fe(CO)_5]_t$ is the amount of $Fe(CO)_5$ left at time t, φ is the photon flux, k_p is the photodissociation rate constant and k_e is the electron dissociative attachment rate constant. Since rate of iron deposition is equal to the rate of $Fe(CO)_5$ depletion and the amount of iron deposited is equal to the amount of $Fe(CO)_5$ dissociated, i.e.,

$$[Fe(s)]_t = [Fe(CO)_5]_0 - [Fe(CO)_5]_t \qquad (V\text{-}2)$$

where $[Fe(CO)_5]_0$ is the initial amount of $Fe(CO)_5$, equation (V-1) becomes:

$$\frac{-d[Fe(CO)_5]}{dt} = \varphi[Fe(CO)_5]_t\left(k_p + k_e\{[Fe(CO)_5]_0 - [Fe(CO)_5]_t\}\right) \qquad (V\text{-}3)$$

The total pressure of the system at time t is given by equation (V-4).

$$P(t) = RT\{5[Fe(s)]_t + [Fe(CO)_5]_t\}$$

or

$$P(t) = RT\{5[Fe(CO)_5]_0 - 4[Fe(CO)_5]_t\} \qquad (V\text{-}4)$$

Integrating equation (V-3) from time 0 to t and solving for $[Fe(CO)_5]_t$ gives:

$$[Fe(CO)_5]_t = \frac{[Fe(CO)_5]_0 \ (k_p + k_e \ [Fe(CO)_5]_0) \ \exp \ -t\varphi(k_p + k_e [Fe(CO)_5]_0)}{k_p + k_e \ [Fe(CO)_5]_0 \ \exp \ -t\varphi(k_p + k_e [Fe(CO)_5]_0)} \qquad (V\text{-}5)$$

Equation (V-4) then becomes:

$$P(t) = RT\left\{5[Fe(CO)_5]_0 - 4\left[\frac{[Fe(CO)_5]_0 \ (k_p + k_e [Fe(CO)_5]_0) \exp. -t\varphi(k_p + k_e [Fe(CO)_5]_0)}{k_p + k_e [Fe(CO)_5]_0 \ \exp \ -t\varphi(k_p + k_e [Fe(CO)_5]_0)}\right]\right\} \qquad (V\text{-}6)$$

If electron dissociative attachment is neglected, equation V-6 becomes:

$$P(t) = RT\{5[Fe(CO)_5]_0 - 4[Fe(CO)_5]_0 \ \exp \ -t\varphi k_p\} \qquad (V\text{-}7)$$

Fig. V-6 is a plot of the increase in pressure vs. time using equation (V-7) and a starting pressure of 2.60 millitorr. In this case only photodissociation occurs. Fig. V-7 is a plot of the increase in pressure vs. time using equation (V-6) and a starting pressure of 2.60 millitorr. Comparing these two plots one can see that for only photodissociation the curve is convex, whereas, for both photodissociation and electron dissociative attachment the curve begins concave and then turns over. This trend was observed in all the experimental plots obtained (see Fig. V-5). This suggests that EDA and photodissociation were both involved in forming the iron films. Because of the instability of the Hg/Xe lamp, the absolute value of the photon flux was an unknown, and k_e could not be obtained.

An interesting experiment for the future would be to use a stable source of monochromatic light in the region of 2537 Å. This would be below the photodissociation threshold of $Fe(CO)_5$ but above the photoelectric threshold of soda glass. From this a value for k_e could easily be obtained.

REFERENCES FOR CHAPTER V

1. L.L. Baker, Jr. and R.B. Bernstein, J. Am. Chem. Soc., 73,4434 (1951).
2. E.G. Derouane, J.B. Nagy, and M. van Eenoo, J. of Cat., 58, 230 (1979).
3. T.F. Deutsch, D.J. Ehrlich, and R.M. Osgood, Jr., J. Appl. Phys. Lett., 35(2), 175, (1979).
4. V.K. Rohatgi, J. Appl. Phys. Lett., 28(9), 951, (1957).
5. A. Becuchamp and S. George, Thin Films, (1980).
6. L. Hellner, J. Masanet, and Vermeil, Nouveau Journal de Chemie, 3, 721, (1979).

Figure V-1. Schematic diagram of experimental apparatus

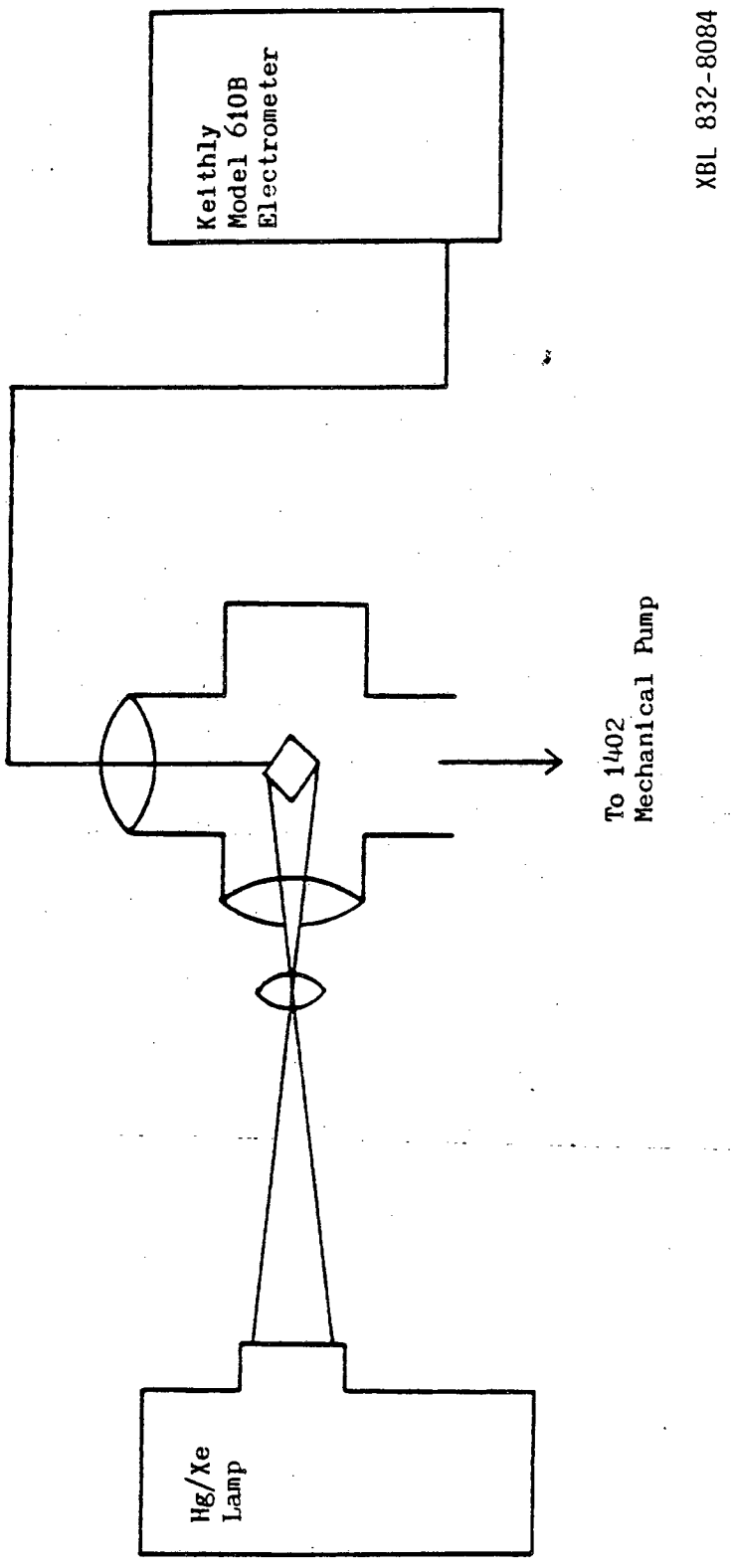
Keithly
Model 610B
Electrometer
To 1402
Mechanical Pump
Hg/Xe
Lamp
XBL 832-8084

Fig. V-1

Figure V-2. Schematic diagram of experimental apparatus

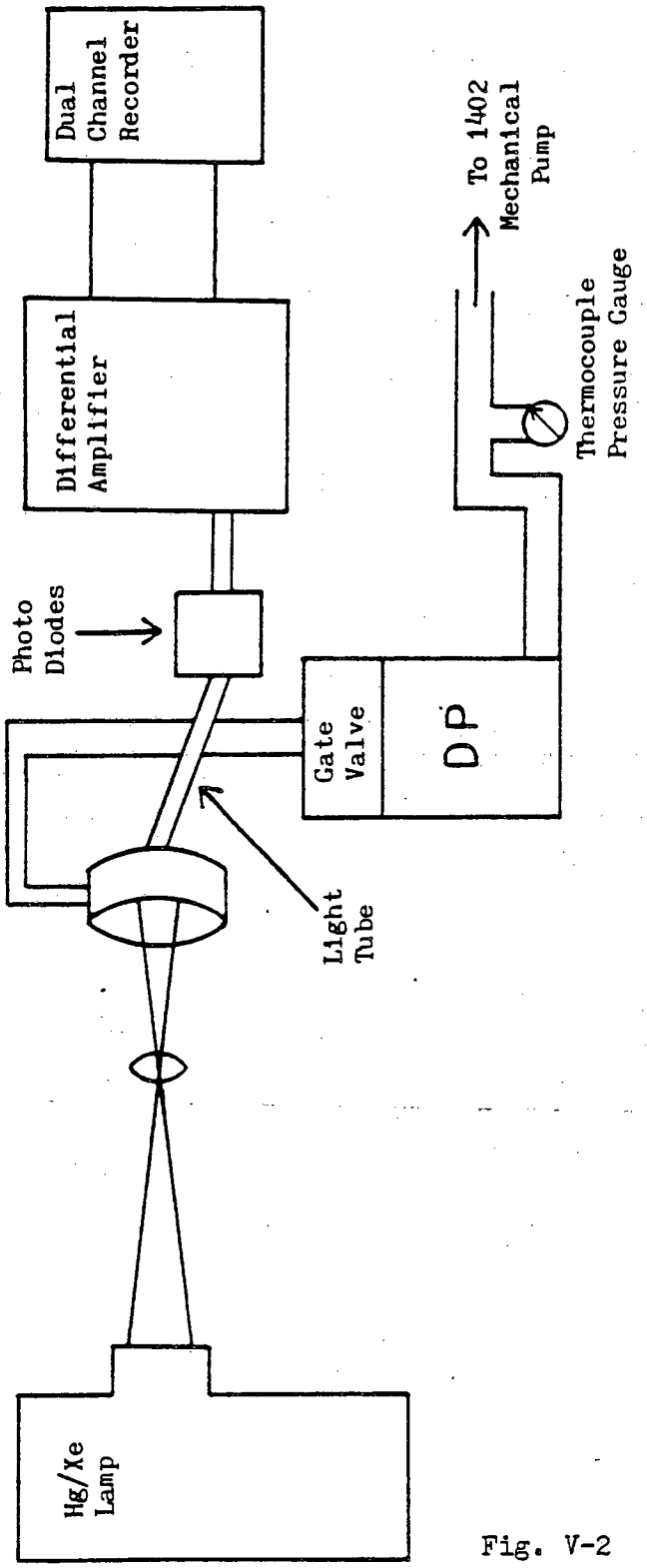
Dual Channel Recorder
Differential Amplifier
Photo Diodes
Gate Valve
DP
To 1402 Mechanical Pump
Thermocouple Pressure Gauge
Light Tube
Hg/Xe Lamp
XBL 832-8083

Fig. V-2

Figure V-3. Diagram of sample cell

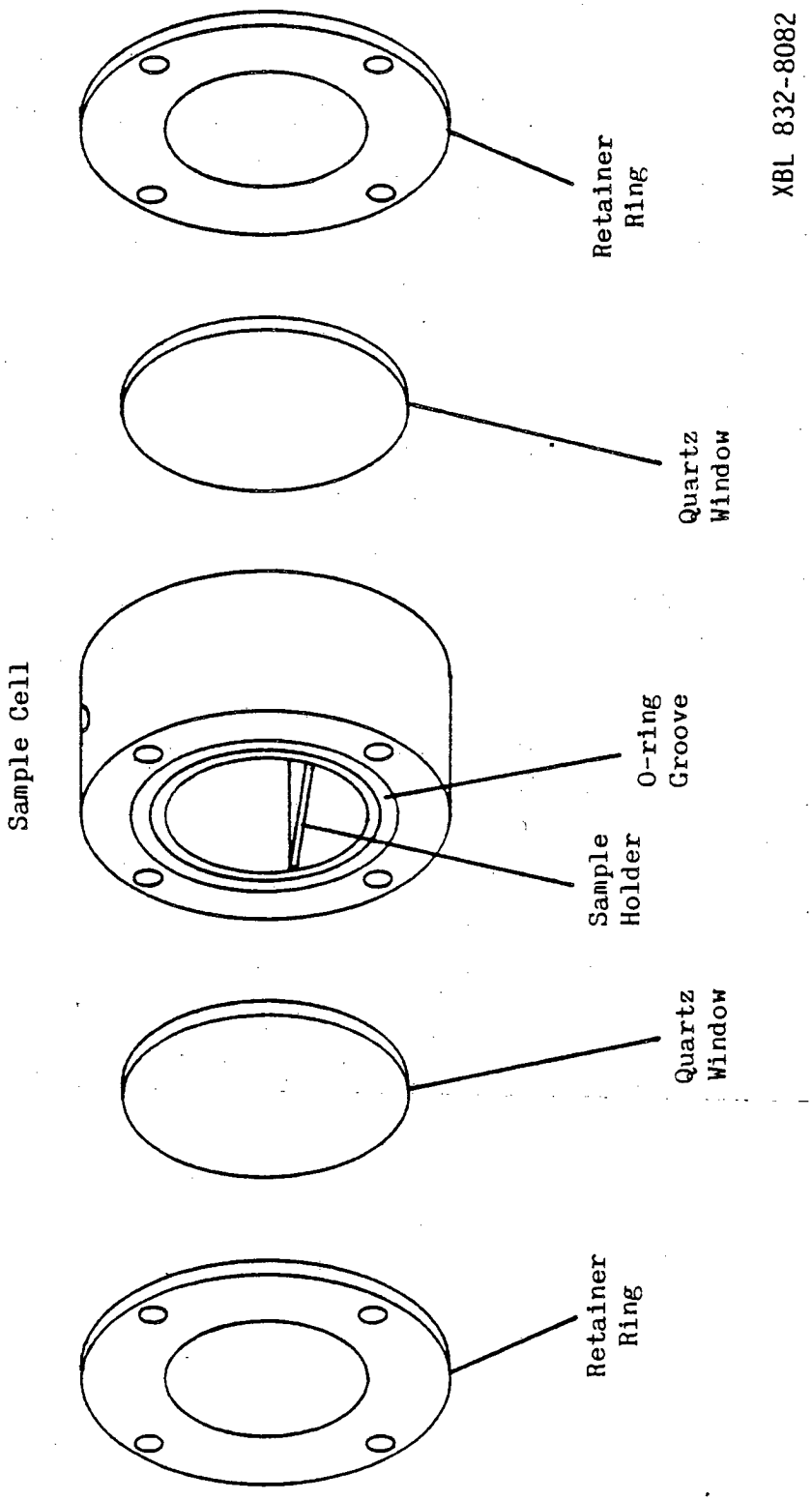
Retainer Ring
Quartz Window
Sample Cell
O-ring Groove
Sample Holder
Quartz Window
Retainer Ring
XBL 832-8082

Fig. V-3

Figure V-4. Diagram of modified experimental apparatus

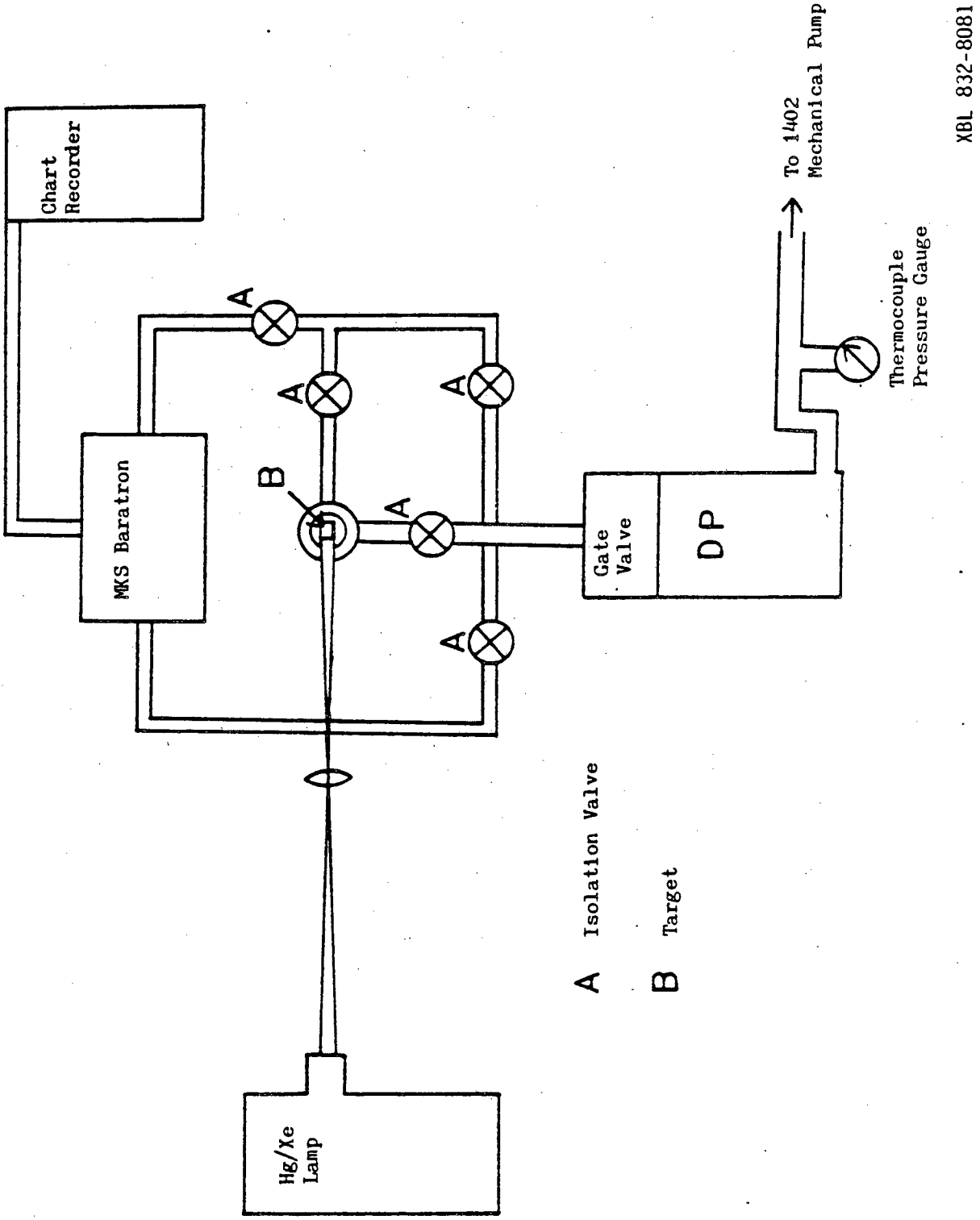
Chart Recorder
MKS Baratron
Hg/Xe Lamp
A
B
Gate Valve
DP
To 1402 Mechanical Pump
Thermocouple Pressure Gauge
A Isolation Valve
B Target
XBL 832-8081

Fig. V-4

Figure V-5. A typical plot of the increase in pressure vs. time

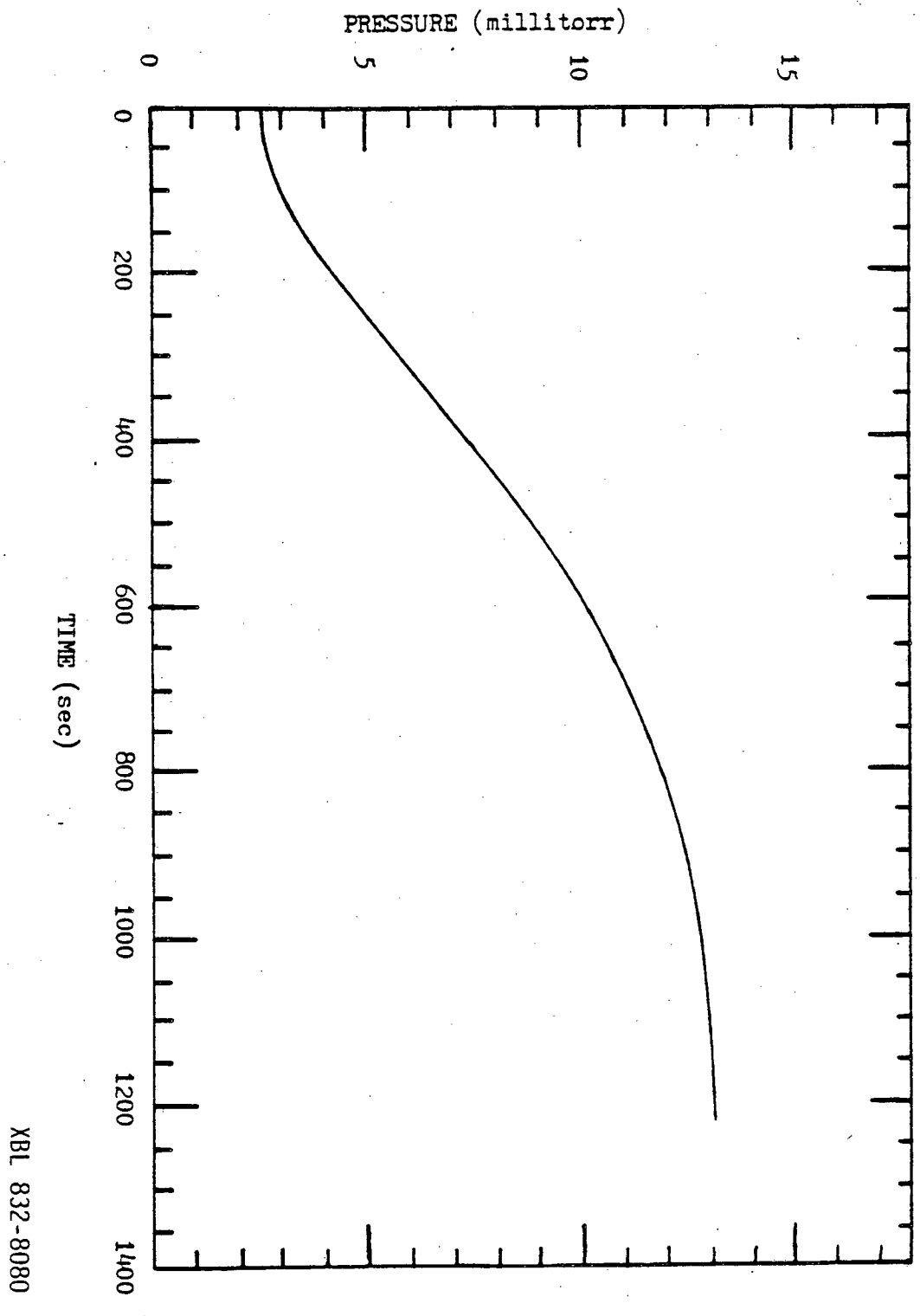
PRESSURE (millitorr)
0
5
10
15
TIME (sec)
0
200
400
600
800
1000
1200
1400
XBL 832-8080

Fig. V-5

Figure V-6. Calculated plot of only photodissociation

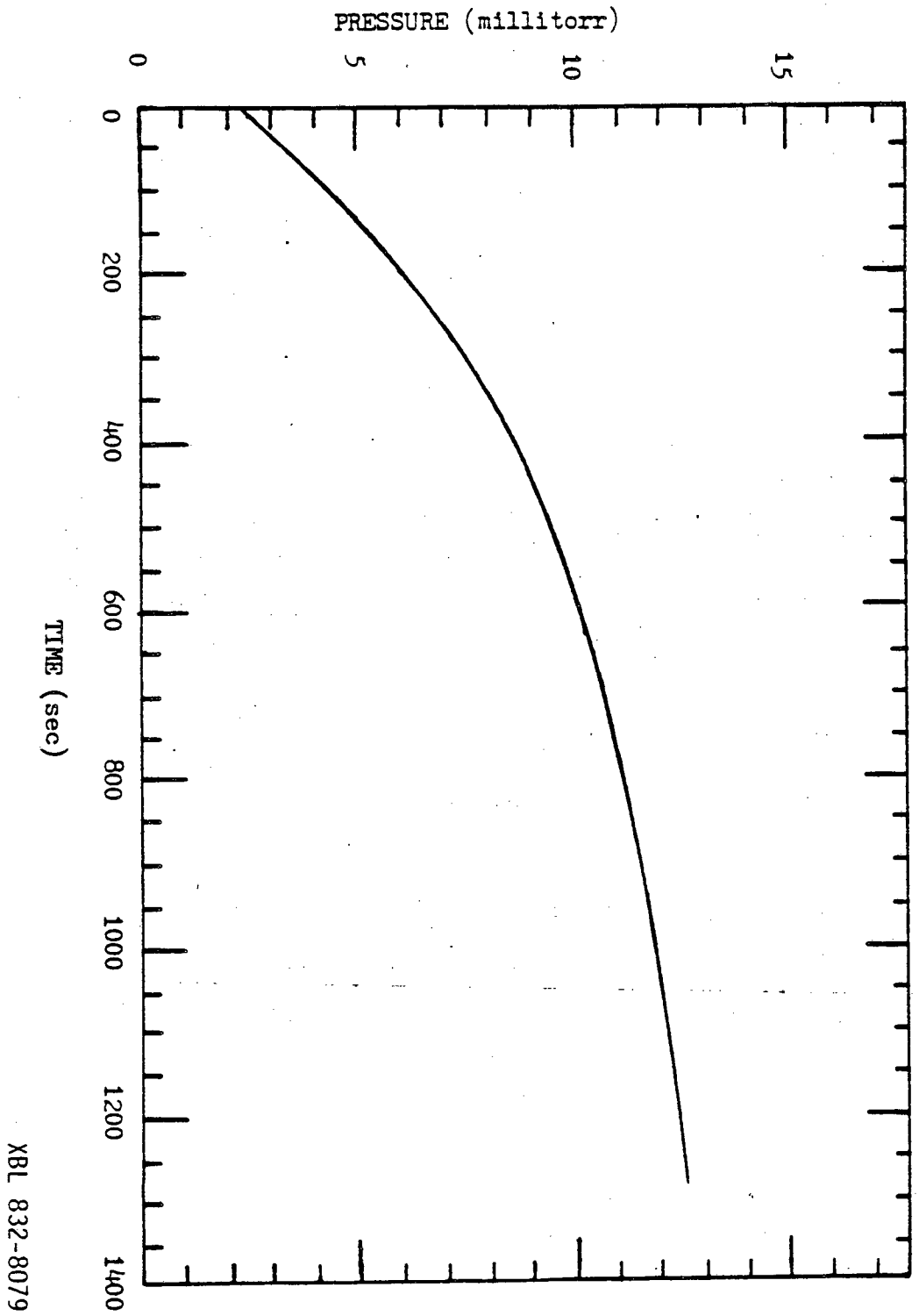
PRESSURE (millitorr)
0
5
10
15
0
200
400
600
800
1000
1200
1400
TIME (sec)
XBL 832-8079

Fig. V-6

Figure V-7. Calculated plot of photodissociation and electron dissociative attachment

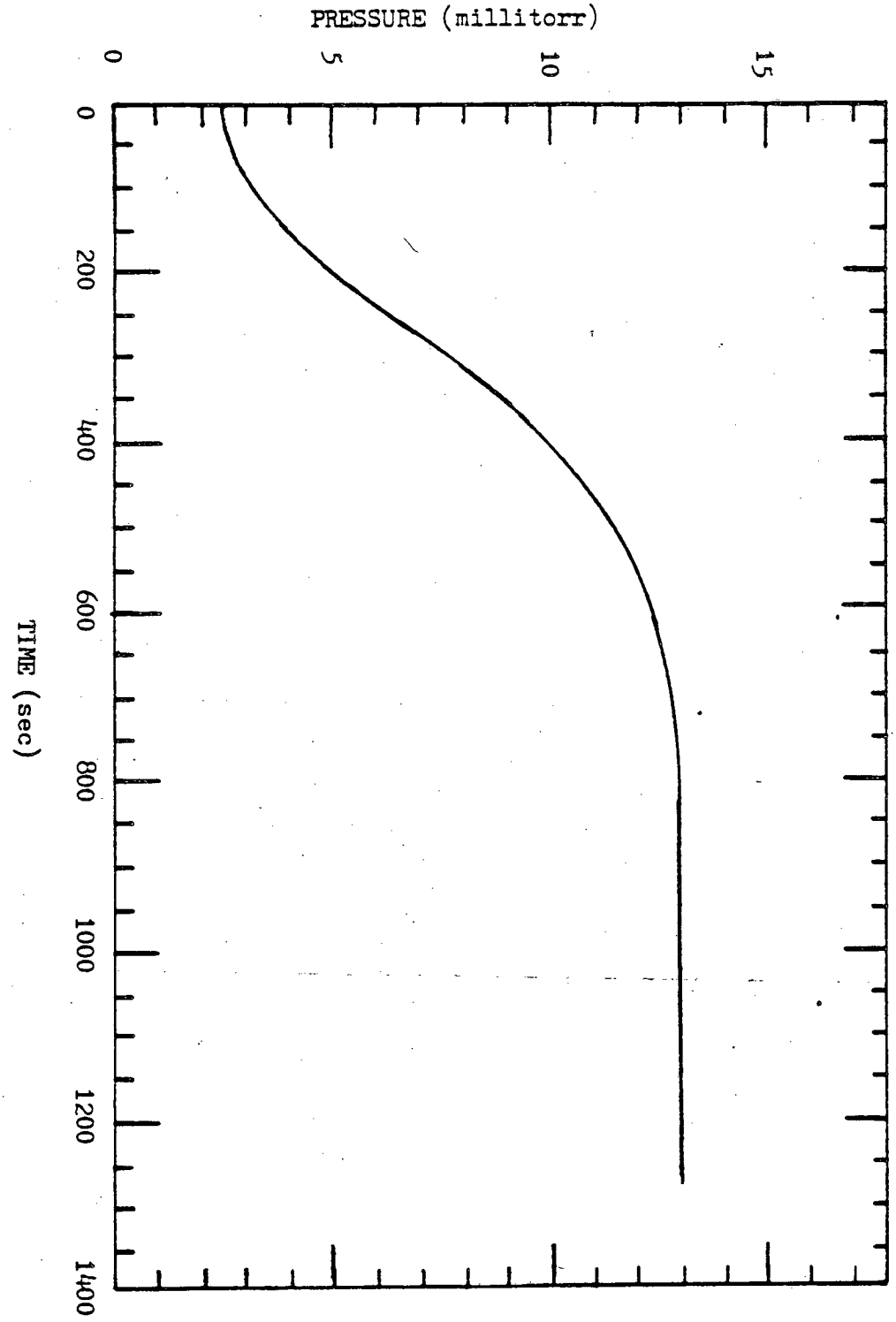
PRESSURE (millitorr)
0
5
10
15
TIME (sec)
0
200
400
600
800
1000
1200
1400
XBL 832-8078

Fig. V-7

This report was done with support from the Department of Energy. Any conclusions or opinions expressed in this report represent solely those of the author(s) and not necessarily those of The Regents of the University of California, the Lawrence Berkeley Laboratory or the Department of Energy.

Reference to a company or product name does not imply approval or recommendation of the product by the University of California or the U.S. Department of Energy to the exclusion of others that may be suitable.

TECHNICAL INFORMATION DEPARTMENT
LAWRENCE BERKELEY LABORATORY
UNIVERSITY OF CALIFORNIA
BERKELEY, CALIFORNIA 94720